

Cold Gas Dynamic Spray technology: a comprehensive review of processing conditions for various technological developments till to date

R.N. Raelison<sup>a\*</sup>, Y. Xie<sup>a</sup>, T. Sapanathan<sup>b</sup>, MP. Planche<sup>a</sup>, R. Kromer<sup>a</sup>, S. Costil<sup>a</sup>, C. Langlade<sup>a</sup>

<sup>a</sup> Laboratoire Interdisciplinaire Carnot de Bourgogne - Site UTBM, UMR 6303 CNRS, Université de Bourgogne Franche-Comté UTBM, 90100 Belfort, France

<sup>b</sup> Institute of Mechanics, Materials and Civil Engineering, Université catholique de Louvain, B-1348 Louvain-la-Neuve, Belgium

\* Corresponding author: rija-nirina.raelison@utbm.fr (+33 678749153)

## Abstract

Today, cold gas dynamic spray (CGDS) technology has thrived with considerable capabilities for manufacturing various technological depositions. The deposition conditions have been developed through many years and that have led to produce ample experimental data which is available in the literature. But, recent research and development activities also reveal innovative findings regarding various deposition conditions. This paper contains a review of experimental deposition procedures for the cold spray additive manufacturing. Details of processing conditions are reported and classified into various categories of baseline working conditions, specific processing including deposition of nanotechnological components, composites-based structures and hybrid coating with substrate deposition. Available substrate treatments and their contributions on the deposition capability were also included. A large collection of experimental data from the literature is addressed in the Appendices A1-A6.

**Keywords:** cold spraying; processing conditions; advanced materials; experimental database

## Table of contents

Nomenclature .....	2
1. Introduction: developments and capabilities of CGDS technology .....	4
2. Characteristics of the CGDS process .....	6
2.1 Process behaviour and main working parameters .....	6
2.2 In-flight characteristics of the particles .....	7
2.3 Parameter requirements for an adhesion .....	8
3. The baseline working conditions used in cold spraying method.....	9
3.1 Usual conditions for the propellant gas .....	10
3.2 Typical size of the cold spray particles .....	11
4. CGDS manufacturing of advanced coatings .....	12
4.1 Composite-based deposits .....	12
4.2 Nanotechnological deposits.....	13
4.3 Hybrid coating/substrate deposition .....	14
5. Substrate treatment and its contributions .....	16
5.1 Effects of surface roughening on the adhesive behaviour.....	16
5.2 Effects of substrate heating on the adhesive behaviour .....	17
5.3 Effects of surface texturing on the adhesive behaviour .....	18

6. Prospective improvements based on the powder features.....	18
6.1 Effect of temperature of the powder.....	19
6.2 Effect of morphology of the powder.....	19
6.3 Effect of the inner architecture of the powder.....	20
7. Conclusions and future perspectives .....	21
Appendices: comprehensive review of CGDS processing data .....	43
A1. Deposit with a single powder .....	43
A2. Composites-based deposits.....	48
A3. Nanostructured deposits using nanocrystalline powders.....	52
A4. Nanoporous deposits using nanosized powders .....	53
A5. MMCs deposits with nanosized phases .....	54
A6. Hybrid deposit/substrate combinations .....	55
References .....	24

## Nomenclature

### Latin-script symbols

a,b	Dimensionless number	(-)
$d_p$	Particle diameter	(m)
A	Radial cross section of the nozzle	(m <sup>2</sup> )
$A_e$	Radial cross section of the nozzle outlet	(m <sup>2</sup> )
$A_i$	Radial cross section of the nozzle inlet	(m <sup>2</sup> )
$A^*$	Radial cross section of the nozzle throat	(m <sup>2</sup> )
r	Nozzle radius along the nozzle axis	(m)
$r_e$	Radius of nozzle exit	(m)
$r_{throat}$	Radius of nozzle throat	(m)
$d_{throat}$	Diameter of nozzle throat	(m)
z	Coordinate of nozzle axis	(m)
C	Drag coefficient of particle	(-)
$C_p$	Specific heat	(J.kg <sup>-1</sup> .K <sup>-1</sup> )
$L_{div}$	Length of nozzle supersonic part	(-)
M	Mach number	(-)
P	Gas pressure along the nozzle axis	(Pa)
$P_0$	Input stagnation pressure of the propellant gas	(Pa)
Pr	Prandtl number	(-)
Q	Flow rate of particles	(kg.s <sup>-1</sup> )
$R_s$	Specific gas constant	(J.kg <sup>-1</sup> .K <sup>-1</sup> )
Ra	Roughness	(m)
Re	Reynolds number	(-)
$Re_{p0}$	Reynolds number of particle for $\rho = \rho_0$	(-)
SoD	Standoff distance (distance nozzle exit – substrate)	(m)
T	Gas temperature along the nozzle axis	(K)
$T_0$	Input stagnation temperature of the propellant gas	(K)
$T_m$	Melting temperature of particle	(K)
$T_i$	Impact temperature of particle	(K)

$T_R$	Reference temperature (ambient temperature)	(K)
$V$	Gas velocity along the nozzle axis	(m.s <sup>-1</sup> )
$V_{cr}$	Critical velocity of particle for adhesion	(m.s <sup>-1</sup> )
$V_i$	Impact velocity of particle	(m.s <sup>-1</sup> )
$V_{nozzle}$	Velocity of nozzle displacement	(m.s <sup>-1</sup> )

---

#### Greek-script symbols

---

$\gamma$	Ratio of specific heat	(-)
$\epsilon$	Ratio of nozzle sections ( $r_{exit}/r_{throat}$ )	(-)
$\lambda$	Thermal conductivity	(W.m <sup>-1</sup> .K <sup>-1</sup> )
$\mu$	Dynamic viscosity	(kg.m <sup>-1</sup> .s <sup>-1</sup> )
$\rho$	Specific mass (density)	(kg.m <sup>-3</sup> )
$\rho_0$	Initial density of the propellant gas	(kg.m <sup>-3</sup> )
$\sigma_u$	Ultimate yield strength	(Pa)

---

#### Abbreviations

---

ABS	Acrylonitrile Butadiene Styrene
AIISI	American Iron and Steel Institute
BMG	Bulk Metallic Glass
cBN	Cubic Bore Nitride
CFD	Computational fluid dynamics
CGDS	Cold Gas Dynamic Spray
CFRC	Carbon Fibre Reinforced Composite
CNT	Carbon Nanotube
CTE	Coefficient of Thermal Expansion
DBC	Direct Bonded Copper
DSSC	Dye sensitive solar cell
FTO	Fluorine doped Tin Oxide
DE	Deposition Efficiency
GFRC	Glass Fibre Reinforced Composite
HA	Hydroxyapatite
HDPE	High-Density Polyethylene
HRTEM	High Resolution Transmission Electron Microscopy
ITO	Indium Tin Oxide
LPCS	Low pressure cold spraying
LZT	Lead Zirconate Titanate
MMC	Metal Matrix Composite
MWCNT	MultiWall Carbon NanoTube
ND	NanoDiamond
NPDS	NanoParticle Deposition System
PA	Polyamide
PC	Polycarbonate
PEEK	Polyetheretherketone
PEG	Polyethylene glycol
PES	Polyether Sulfone

PET	Polyethylene Terephthalate
PVDF	Polyvinylidene fluoride
PMC	Polymer Matrix Composite
PP	Polypropylene
PPA	Polyphthalamide
PPSU	Polyphenylsulfone
PS	Polystyrene
PSU	Polysulfone
PTFE	Polytetrafluoroethylene
PU	Polyurethane
PVC	Polyvinyl Chloride
SEM	Scanning Electron Microscopy
SoD	Standoff distance
SS	Stainless Steel
WC	Tungsten Carbide
Subscript symbol	
g	Gas
nc	nanocrystalline
np	nanoporous
ns	nanosized
p	Particle

## 1. Introduction: developments and capabilities of CGDS technology

Cold spraying is an innovative additive manufacturing method and it has recently become a promising technique in the material processing field. Primarily, cold spraying is a powder deposition method and it exploits the self-consolidation capability of the solid particles which join together while they retain in their solid state. A high velocity impact enables such self-consolidation capability that is governed by a solid state bonding. This technique was developed in the early twentieth century by Thurston [1]. Later, a blast or a pressurized gas was used to accelerate metallic powders to a maximum velocity of about 300 m/s and subsequently, the high speed collision onto a substrate produces a deposit. In 1950s, a major innovation appeared with a new development made by Rocheville, using a gas flow through a De Laval nozzle which enables to reach higher velocities than those obtained with the existing methodologies at that time, and which produces a uniform thin coating. In the 1980s, the phenomenological behaviour of the cold spray method has been further investigated by the Institute of Theoretical and Applied Mechanics of the Russian Academy of Science [1,2]. Their findings led to the development of new patents of cold spray devices and experimental procedures of the cold spray manufacturing process that eventually results as a reliable additive processing technique. Although, several feasibility studies demonstrate the viability of cold spraying, the mechanisms of deposit formation and bonding are continuously being investigated to expand the applicable materials.

The deposition during a cold spray process is mainly governed by two steps including an adhesion of the particles on a substrate and a growth of the deposit. Each step has been characterized by distinct phenomena of bonding mechanisms. Regarding the deposit growth,

interparticle cohesion due to a plastic deformation is suggested for ductile materials such as metals. The interfacial cohesion is believed to occur by atomic bonding due to an intimate contact or by metallurgical bonding due to phase transformations, while the interface is subjected to the collision and severely experiences a high strain rate plastic deformation [3–5]. In contrast, fragmentation and self-compaction were also identified and the consolidation of the final deposit is resulted from the stacking and interlocking of fragments, especially for non-ductile materials such as ceramics. Successful build-up of coating has been obtained for various oxides [6–12].

In literature for cold spraying, researchers have shown experimental observations of bonding mechanisms which mainly occur due to metallurgical bonding, mechanical anchoring, mechanical interlocking or interfacial mixing. Metallurgical bonding can be explained as a result of a heteroepitaxy phenomenon which causes dynamic recrystallization [13], or a hyper-quenching phenomenon that occurs due to an interfacial confinement of significantly large plastic strain (adiabatic shearing) and forms an amorphous intermediate layer containing intermetallic phases [14–16]. Mechanical anchoring is caused by a weak indentation of the particles onto the substrate, capable of ensuring anchoring of the particles, and mainly observed for combinations of metallic particles with ceramic substrates [17–19]. Mechanical interlocking corresponds to an embedment of particles on the substrate due to a deep penetration as observed in the following particle/substrate combinations: metal/polymer [20,21], oxide/polymer [22], ceramic/metal [23] and metal/metal [24]. The idea of interlocking can also be extended to the case of mechanical deformation of particles within the geometrical imperfections on the substrate's surface [25,26]. This is also given as an interpretation for the continuity of material across the interface generated during the deposition of soft particles onto a hard substrate. Few examples of such cases are soft metal/polymer [21,25–27], metal/ceramic [19] and polymer/metal [28,29]. Moreover, during an interfacial mixing, the adhesion mechanism is governed by the development of interfacial vortices which allow the particles and the substrate to intermix across the interface [26,30,31].

Since cold spraying allows to deposit a broad range of advanced and new materials, academics and industries show a growing interest in CGDS technology over the last 15 years. The CGDS method provides various functional properties for several existing industrial applications and it is also expected to have substantial progress over the next decades. Today, several material deposits have been developed [32–34]. They can be classified based on their deposition procedure and the type of materials. Thereby, it suggests three distinct categories namely, (1) the deposits produced by the nature of one material, (2) the composites-based deposits made of a mixture of different powders, and (3) the nanotechnological deposits (i.e. a deposit producing nano size features). The flexibility of the CGDS method in terms of adhesion mechanisms also suggests an additional deposit category as material hybridization between the particles and the substrate. In this respect, this additional deposit category considers the fact of hybridization and it can be named as “hybrid deposit/substrate assembly”. Till to date, the later includes the following cases: oxide/ceramic [10,35,36], oxide/polymer [22,37,38], metal/polymer [17,25,28,39], metal/PMCs [25–27], polymer/metal [29,40], metal/ceramic [17–19,41], ceramic/metal [23,37,38,42], and cermet/metal [43–47].

In order to achieve such a wide range of deposits, various deposition conditions have been developed. In this context, viability of different deposition methods was proven and ample experimental data has been produced. Given the current status of the cold spray technology, it is essential that the overall processing conditions are gathered to provide a meaningful database. Therefore, the purpose of this paper is to review those existing experimental deposition

conditions. It also includes a brief description of the cold spray process and its main characteristics (Section 2), and then followed by a description of baseline working conditions (Section 3). Processing conditions of advanced coatings are then reported in Section 4. Section 5 addresses the substrate treatments and their contributions in the efficiency of the cold spray technique. Finally, an appendix provides various processing conditions and a summary of experimental data which covers a broad range of possible depositions.

## 2. Characteristics of the CGDS process

### 2.1 Process behaviour and main working parameters

Fig. 1 shows a schematic illustration of the cold spray process. Due to the pressure difference between the nozzle inlet and the nozzle outlet, a gas flows through the De Laval nozzle at a subsonic velocity within the “converging part”, accelerates to supersonic velocity as the gas expands within the “diverging part”. The nozzle dimensions and the gas pressure, temperature and type determine the gas flow which also governs the in-flight behaviour of the particles. The particles leave the nozzle and form a deposit onto the substrate due to high velocity collision. Thus, it enables to identify the main process parameters of each component specified in Fig. 1, for the nozzle, the propellant gas, the particles and the nozzle outlet conditions. The nozzle is characterized by its dimension, and most importantly the throat section, the exit section and the length of the “diverging part”. This length affects the velocity of the particles. The nozzle expansion ratio (exit section/throat section) is used to determine the Mach number at the exit of the nozzle.

For a given propellant gas, the deposition procedure requires to set the temperature and pressure of the prechamber ( $T_0$  and  $P_0$ ). In terms of powder feedstock, the working parameters are determined by the material type, particle shape, morphology, and granulometry. The standoff distance between the nozzle and the substrate is also a process variable. Generally, a well-defined set of parameters provides the working conditions for a successful deposition. For various coatings, a review of the processing conditions is addressed in the sections 4 and 5, while a comprehensive data collection is also reported in the appendix.

A distinction can be made between the working parameters, particles' in-flight characteristics and substrate treatment. The latter includes the temperature (heated or non-heated) condition and the surface condition in terms of topology (smoothness and texture). The surface texture is a pattern of periodic irregularity on a surface. The texture of the substrate is a new solution that is being explored for its capability to improve the adhesion. A review on the investigation of substrate treatments and their contributions to the deposition capabilities including the effect of the innovative method of texturing<sup>1</sup> are presented in Section 5. The particles' in-flight characteristics are determined by the kinematic behaviour of the particles and the thermal kinetics within the propellant gas flow. Hence, both temperature and velocity of the particles define a critical set of parameters that highly influences the collision and the subsequent adhesion behaviours.

---

<sup>1</sup> (“innovative texturing” is a laser ablation technique that enables producing a pattern of periodic irregularity on a surface)

## 2.2 In-flight characteristics of the particles

During a deposition, in-flight characteristics of particles mainly govern the formation of coating, its growth, and the quality of the final deposit. The state of the particles prior to the collision onto the substrate is generally described using their velocity and their temperature, respectively denoted by  $V_p$  (particles' velocity) and  $T_p$  (particles' temperature). These set of useful parameters can be used to characterize the deposition capability in terms of a deposition window. Moreover, the current technological advances offer the trustworthy measurements of  $V_p$  for the micron-sized particles. In this context, a large number of experimental results are presented in the literature. In many of those previous studies, a DPV2000 laser system was used to characterise the kinematics of particles during the cold spraying method. The literature of the particles' velocity measurement also includes other laser measurement systems such as Laser-2-Focus (L2F) and Particle Image Velocimetry (PIV) while they offer a high spatial resolution [48].

Unlike the particles' velocity ( $V_p$ ), the particles' temperature ( $T_p$ ) is difficult to measure due to their low values and the small particle size, (lower than 100  $\mu\text{m}$ ). Therefore, the particles' temperature prior to the collision is poorly characterized. Alternatively, numerical simulations of the particle/gas interaction combined with the heat transfer over the particles' surface is modelled using a thermal convection with Newton's law, to predict the  $T_p$ . Assuming a uniform convection, the equation of Nusselt number for a sphere exposed to an impinging flow is also used to predict the particle's temperature. Under the conditions of a steady state heat transfer and a uniform temperature distribution within a particle (i.e. that is acceptable due to the small particle size which gives a short heat transfer characteristic time), the particles' temperature variation through the nozzle based on the energy balance of gas flow is given by:

$$\rho_p C_{pp} V_p \frac{dT_p}{dz} = \frac{6\lambda_g}{d_p^2} \frac{Nu}{(T-T_p)} \quad (\text{Eq. 1})$$

where, the parameters of particles and gas are respectively denoted using the subscripts of  $p$  and  $g$ .  $z$  is the axial coordinate along the nozzle. The Nusselt number is commonly defined by Ranz-Marshall correlation (Eq. 2). However, a recent review [48] underlines that there is a few expressions of Nusselt number that suits for various situations such as high particle's Reynolds number [49], high Mach number [50], or including the consideration of boundary layer over the particle's surface [51]. But the accuracy of each correlation has not been completely discussed in the literature of cold spraying [48]. In any case, the Nusselt number depends on the Reynolds number and consequently it depends on the particles' velocity which is formulated based on the Newton's law of coupling the gas flow and the particles' motion (Eq. 3).

$$Nu = 2a + 0.459bRe_{p0}^{0.5}Pr^{0.3a} \quad (\text{Eq. 2})$$

$$\rho_p V_p \frac{dV_p}{dz} = C \frac{3}{4} \frac{\rho}{d_p} (V - V_p)^2 \quad (\text{Eq. 3})$$

where,  $a$  and  $b$  are constants,  $Re_p$  is the Reynolds number obtained using  $V_p$ ,  $Pr$  is the Prandtl number of the gas and  $C$  is the drag coefficient.

An accurate determination of the gas flow requires a computational fluid dynamics (CFD) simulation, but a 1D compressible flow formulation enables to obtain a quick and useful

approximation under the following assumptions: a steady-state flow, an ideal gas, an isentropic and frictionless flow without particles' influence on momentum transfer from the gas to the particle, and having a uniform gas expansion along the nozzle radius. The equations (Eq. 4-6) sequentially compute the Mach number ( $M$ ) that depends on the nozzle radius, gas temperature and gas velocity.

$$\frac{A}{A^*} = \frac{1}{M} \left[ \frac{2}{\gamma+1} \left( 1 + \frac{\gamma-1}{2} M^2 \right) \right]^{\frac{\gamma+1}{2(\gamma-1)}} \quad (\text{Eq. 4})$$

$$\frac{T}{T_0} = \left( 1 + \frac{\gamma-1}{2} M^2 \right)^{-1} \quad (\text{Eq. 5})$$

$$V = M \sqrt{\gamma R_s T} = \frac{M \gamma}{\left( 1 + \frac{\gamma-1}{2} M^2 \right)^{1/2}} (R_s T_0)^{1/2} = f(\gamma) (R_s T_0)^{\frac{1}{2}} \quad (\text{Eq. 6})$$

$$\frac{\rho}{\rho_0} = \left( 1 + \frac{\gamma-1}{2} M^2 \right)^{-\frac{1}{\gamma-1}} \quad (\text{Eq. 7})$$

Fig. 2 shows typical temperature and velocity variances of a cold sprayed particle, depicted on the grid of pressure and temperature of the propellant gas using a 1D computational procedure. Given the large number of process parameters and their mapping, such computations give a useful approximation of particles' in-flight parameters without a long and costly experimental work. Furthermore, the 1D procedure can help to predict and/or to optimise the deposition efficiency while the coupling parameters of adhesion is governed by  $V_p$  and/or  $T_p$ . A summary for the selection of adequate and/or optimum process parameters based on a simple analytical tool is also given in Fig. 3.

### 2.3 Parameter requirements for an adhesion

In literature for cold spraying, there are a limited number of studies on physics of adhesion. At present, the knowledge in this field is limited despite having several detailed studies of bonded interfaces. Different theories were suggested based on interfacial features revealed using various observation methods including scanning electron microscopy (SEM), High Resolution Transmission Electron Microscopy (HRTEM), light microscope and the characterization tools used to describe the physical phenomena. Although, natures of interfaces have been identified, the required specifications of parameters to produce a reliable and predictable adhesion through well-defined process parameters remain unclear. Currently, macroscopic parameters (e.g. the critical velocity of the particle) are suggested to predict the adhesion. Two generic models were developed using shear instability phenomenon similar to that observed during an explosive welding. The literature on explosive welding method provides significant experimental and numerical studies which confirm the necessity of the shear instability condition to produce a successful welding using Kelvin-Helmholtz instability model. A model for adhesion was also similarly developed, particularly for metal combinations [4]. Assadi *et al.* have found the following correlation for the critical bonding velocity [4]:

$$V_{cr} = 667 - 0.014\rho + 0.08T_m + 0.1\sigma_u - 0.4T_i \quad (\text{Eq. 7})$$

where,  $\rho$ ,  $\sigma_u$ ,  $T_m$  and  $T_i$  respectively denote material density ( $\text{kg.m}^{-3}$ ), ultimate tensile stress (MPa), melting temperature ( $^{\circ}\text{C}$ ), and impact temperature ( $^{\circ}\text{C}$ ). Another generic model was developed by Schmidt *et al.* for the particle size larger than  $25 \mu\text{m}$  [52]. Their critical velocity formulation based on correlations between the particle's kinetic energy, material strength, and heat generation due to the plastic deformation, is given by [52]:

$$V_{cr} = \frac{1}{2} \left[ \left\{ \frac{16\sigma_u}{\rho(T_m - T_R)} \right\} (T_m - T_i) \right]^{\frac{1}{2}} \quad (\text{Eq. 8})$$

where,  $c_p$  is the specific heat capacity of the material and  $T_R$  is the reference temperature (ambient temperature usually).

Computing the ratio of  $V_p/V_{cr}$  for different sets of process parameters can help to identify the deposition window, but it only predicts the deposition rather than the bond quality. Unlike this ratio, a deposition efficiency (DE) model can provide a more accurate prediction of the deposition. Fig. 4 demonstrates a typical comparison between these two approaches. The DE is computed using a linear model based on particles' velocities characterized by Alkimov *et al.* [53]. Generally, DE computations are more reliable using a model based on experimental measurements. But, ample characterizations of the particles' behaviour and viable correlations governed by the process parameters are required to make a DE model to be well predictive. Ongoing investigations are promising to fundamentally increase the prediction capability of the CGDS process; nevertheless reliable models have to be developed to realize such radical achievements. Although, empirical correlations of the DE have been established [54–56], they cannot predict the DE over a wide range of materials and process conditions because those existing empirical approaches are very restrictive. However, the empirical models can help to identify the deposition capability of the CGDS method using the particles' in-flight parameters which can be determined by the parameters of propellant gas using the equations of the gas flow and particles' interaction [57].

### 3. The baseline working conditions used in cold spraying method

The cold spray process involves numerous parameters since the deposition is determined by the properties of the propellant gas, particles' characteristics, nozzle dimensions, nozzle outlet conditions and substrate treatment. These parameters are interdependent, thus an experimental selection of the accurate parameters becomes a difficult task. In addition, there are no available conventional standards for cold spraying until today. However, a good cold spray protocol such as MIL-STD (US military standard) provides a high level guidance for the cold spray process.

Generally, the practice of using low temperature and pressure distinguishes the CGDS process from the conventional thermal spraying processes. The information presented in this work provides a better depiction of CGDS process conditions and a construction of a reliable database. It also reports deposition conditions of a powder feedstock of various materials. Furthermore, this review represents the majority of the work available in the literature of cold spraying, and provides the useful deposition conditions as a guideline which can be used as a reliable baseline for a selection of the process parameters.

### 3.1 Usual conditions for the propellant gas

Helium (He) or nitrogen (N<sub>2</sub>) or air is used as the main process gas in cold spraying. Helium remains the most efficient gas due to its high specific gas constant and low molecular weight compared to N<sub>2</sub> and air as shown in Table 1. Eq.6 also clearly shows the dependency of the gas velocity on the specific heat ratio ( $\gamma$ ) and the specific gas constant ( $R_s$ ). According to Eq. 4-6, the Mach number and the term  $f(\gamma)$  are weakly influenced by  $\gamma$  for its range between 1.4-1.66 (Fig. 5). Thus, among those three gases, the significant change in velocity results from  $R_s$ , or from the term  $R_s T_0$ . Fig. 5 depicts the gas velocity based on both nozzle expansion ratio and  $R_s T_0$  for the  $R_s$  range of 200-2000 J.kg<sup>-1</sup>.K<sup>-1</sup> and  $T_0$  value of 293K (i.e., considering a non-heated gas). The velocities of N<sub>2</sub> and air are very limited due to their low  $R_s$  values whereas He produces high velocities which subsequently result with better efficiency than that of using other gases (Fig. 6). Basically, the particles' velocity depends on the gas flow (i.e. it is governed by the velocity and the density of the propellant gas) whose evolution is described by  $\gamma$ . For a given  $\gamma$  between 1.4-1.66, the effect of  $\gamma$  on the gas density is also weak (Fig. 6a). These general correlations show that the specific gas constant is an important parameter of the gas which determines the velocity efficiency for both propellant gas and particles. That is, the particles can easily reach high impact velocities while using the helium gas (Fig. 6b).

He is recommended for costly materials and for metals that require to reach high critical velocities [58]. In addition, He offers other advantages such as increase in working temperature, increase in productivity, and improvement in densification of the deposits [58–60]. Although He is beneficial to obtain an efficient deposition, it is not an economically viable solution. N<sub>2</sub> is more affordable than He, and air can be freely supplied from a compressor. Therefore, both N<sub>2</sub> and air are widely used to reduce the manufacturing cost. N<sub>2</sub> also prevents the samples from oxidation compared to the air.

Fig. 7 shows the characteristic pressure and temperature of the propellant gas for various materials which require pressures of up to 5MPa. The preheating temperature of the gas is normally between 20 - 800°C. Specific details of the preheating temperatures are reported in the Appendix (Table A1). For instance a high temperature range (500°C-850°C) is required to deposit cermets such as MCrAlY compound and nickel based alloys. Deposition of ceramics and oxides requires low temperature and low pressure conditions (typically <300 °C, and <2 MPa). Deposition of nickel alloys requires high pressure (up to 4MPa). Fig. 8a shows that the low temperature and low pressure are suitable for soft metals such as zinc and tin. Deposition of relatively hard metals (e.g. copper, aluminium, titanium) can be performed under similar conditions using He. N<sub>2</sub> or air requires increase in both gas pressure and temperature (Fig. 8b). Successful depositions of stainless steel or titanium based alloys are also performed at high temperature and high pressure (Fig. 8c).

During the cold spray process, the inlet pressure and the inlet temperature of the propellant gas generally affects the kinematics of the particles. The carrier gas has the main function to inject the particles inside the nozzle. For this purpose, the injection pressure and the injection temperature of the carrier gas do not require to be very high (i.e. similar to the inlet pressure-temperature of the propellant gas). However, an increase in the pressure and/or temperature of the carrier gas contributes for an increase of gas pressure and temperature within the nozzle's convergent zone. With this cumulative effect, it enables the particles to reach high velocities and high temperatures. This situation improves the deposition efficiency and the bonding strength of the deposit [61]. However, additional pressure resulted from the carrier gas can also have an adverse effects on the kinematics of the gas flow, particularly when the temperature of

the carrier gas is lower than the temperature of the propellant gas. The mixing of those gases with such a temperature difference decreases the gas temperature at the upstream of the nozzle throat, and then it limits the kinematic capability of the propellant gas due to the drop in temperature due to the mixing of temperatures. Moreover, the particles' deposition becomes less efficient, especially when the injection pressure of the carrier gas promotes the mixing of temperatures [62].

### 3.2 Typical size of the cold spray particles

In practice, the effectiveness of the cold spray deposition depends on the size of the particles. A range of particles' sizes below 100  $\mu\text{m}$  in diameter is generally used while particles with larger diameters (i.e.  $\geq 100 \mu\text{m}$ ) are difficult to accelerate. Thus, extra care must be taken when selecting the particles' sizes. Generally, there exists an optimum range of particles' sizes above which there can be a reduction in the particles' velocity and consequently in the deposition efficiency. Equations 1-7 (Eq.1-7) can be used to assess the viability of the deposition based on the capability of a cold spray system and the geometry of a nozzle. In the literature, the maximum particle size varies in between 20-60 $\mu\text{m}$  for several materials, except aluminium (known as a light metal) and zinc (known as a soft metal) have been used with up to 100 $\mu\text{m}$  and 90 $\mu\text{m}$ , respectively (Fig. 9). But the optimum deposition efficiency also relies on the granulometry of the particles. For a given particle size distribution denoted by  $f(d_p)$ , Assadi *et al.* suggested that the deposition efficiency (DE) is defined by the following equation:  $DE = \int_0^{\infty} f(d_p) dd_p$  [63].

The selection of the suitable granulometry requires the information of the optimum particle size. Even though equations 1-7 (Eq.1-7) enable to find the upper limit of the particles' sizes, they cannot be used to identify the lower limit since the particles with small diameters become very sensitive to the heating within the nozzle's throat zone, thermomechanical sticking phenomenon on the nozzle's inside wall, flow deviation near the substrates or due to the bow shock effect within this zone (the zone near the substrate). In order to overcome these limitations, Chun *et al.* suggested a specific nozzle design that was used to deposit 5  $\mu\text{m}$  copper particles using usual temperature and pressure conditions of the propellant gas [64]. Significant increase in the DE, adhesion strength and coating thickness were obtained in their experiments. But, the deposition was poor when fine particles are used with a conventional nozzle [64]. In addition, fine particles can suffer from self-agglomeration that may cause some issues associated with the gas flow. Hence, finding the minimum particle size requires a complex assessment which should include the limiting behaviour of the deposit formation. In this review, a collection of experimental results with various particles' sizes is provided in Fig. 9 and several successful cold spray tests are reported in Section 5.

Some studies also investigated the deposition of submicron sized powders [10,12,37,38,65,66]. A very low pressure and low temperature condition was used in those studies for majority of successful depositions for the particles' size between 20nm-1 $\mu\text{m}$ . A vacuum deposition is generally performed and the particles are accelerated by a non-heated gas inside a nozzle specifically designed for such submicron powders. This cold spray method can also be used for the manufacturing of a fine porous structure and for the coating of thermally sensitive materials. Details of this innovative feature are reported in Section 4.2.

#### 4. CGDS manufacturing of advanced coatings

Current focus of cold spray method is to develop the process parameters for depositing composite-based coatings and the use of nanosized powders. The processing conditions of these materials require advanced proficiency in the cold spraying technique. This section reports the various methods of composite-based depositions suggested in the literature. Very limited literature is available on CGDS manufacturing of nanotechnological deposits. The experimental procedures below provide an overview of the diverse methods used for the deposition of the nanosized powders.

##### 4.1 Composite-based deposits

Basically, typical cold spray conditions are used to deposit the composite-based powders. The main working parameters are not noticeably different for both a single powder deposition and a composite one. The propellant gas working conditions remain same as the usual one while conventional nozzles are also suitable for the composite-based deposits. Prior to the spraying, the dissimilar powders are mixed to provide a composite feedstock. The starting mixture ratio can be adjusted to get the mixed ratio of the deposit. Such preparation is specified in the literature but some studies prefer the use of commercially available mixtures. The powder mixture is fed into the nozzle and sprayed on a substrate. Finding the effective operating conditions may be difficult with this deposition method especially when the dissimilar combination includes a large variation in their mechanical properties. The deposition conditions can be favourable to the adhesion of one material of the mixed powder feedstock while it can be unsuitable for the other. To overcome this difficulty, deposition of an agglomerated mixture was suggested. Strong mechanical mixing followed by a grinding operation is used to produce a powder feedstock made of composite agglomerates. For a dissimilar combination of hard and soft materials such as ceramic/metal, the metal component within agglomerate can act as a binder and facilitates the bonding. An appropriate selection of metallic combinations of soft and hard materials can also prevent the damage of the hard material [67]. For instance, copper particles can confer a buffer function to avoid the cracking of diamond particles during deposition. Moreover, deposition of pre-mixed powders enables to provide thick metal-diamond composite coating [67,68]. Generally, for any pre-mixed feedstock, deposition is performed using typical cold spray process conditions.

Regarding the simultaneous deposition of non-agglomerated composite powders, Sova *et al.* have suggested an alternative method [69,70]. Accordingly, the powder mixing prior to the deposition is no longer a prerequisite. In their method, different powder feedstocks (each feedstock consists of a single powder material) are separately connected to the nozzle [71]. The locations of the injection are determined based on the characteristics of the powder feedstocks. This arrangement provides the suitable in-flight characteristics for each powder material. Finite element computations were also used to determine the location of the injection. Hence, different powders are mixed inside the nozzle while each of them can simultaneously reach their optimal adhesion conditions during the spraying process. For the cases of multi-metallic mixtures, Sova *et al.* suggested that the easily processable powders (aluminium, copper, zinc, ...) were fed in the supersonic part of the nozzle, and the difficult ones (requiring higher temperature) were fed in or near the subsonic section [69, 70]. In case of a metal-ceramic mixture, the subsonic part is suitable for the injection of the metallic powder when a heating of particle is required. An injection of the ceramic powders in the supersonic part prevents the damage of the nozzle throat due to erosion. The flow rate of each injection feedstock is a main parameter to be adjusted since the mixture ratio within the final deposit mainly depends on the flow rate. Several

metal/metal or metal/ceramic composite-based deposits are successfully produced using this method (see Table A2 in the appendix for additional details).

The selection of material combination and the mixture ratio are important tasks. Selection criteria for the deposition of metal matrix composites (MMCs) were reported by Ibrahim *et al.* [72]. The review of Ibrahim *et al.* includes the guidelines that can help to identify a suitable combination of both materials and the ratio of each component. The rule-of-mixture law is also used to predict the property of an MMC deposit. Examples of predictive models for the thermal conductivity and the Young's modulus can be found in [72]. The researchers also identified that the tensile properties of the MMCs (i.e. the yield strength and ultimate strength) increase with the volume fraction of the reinforcements, while decreases in ductility and fracture toughness were noticed [72]. For instance, the elongation of MMCs is reduced tenfold with 10% of reinforcement and it even becomes extremely low (~ 1%) with 20% of reinforcement. As a result of this, beyond a critical ratio of 40% reinforcement, brittle fracture could occur.

#### 4.2 Nanotechnological deposits

The cold sprayed nanotechnological deposits can be classified into three major categories: (1) nanocrystalline media obtained from nanocrystalline powders [43,73–80], (2) deposits made of nano-scaled constituents such as nanoparticulates or carbon nanotubes (CNTs) [81–85], and (3) nano-architectural deposits obtained using nanoporous powders [10,35,65,66,86]. This classification is suggested based on the manufacturing perspective. Details of the process parameters of these classifications are reported in Tables A3 - A5 in the appendix.

The nanocrystalline powders for cold spraying are generally produced using ball milling. These powders are in micron size so that their deposition can be achieved in the same way as suggested for the usual powders. Similar gas conditions are also recommended, despite of the mechanical property differences between these two powder types (nanocrystalline powder and usual powder). The usual deposition conditions provide both the adhesion and consolidation for several metallic powder feedstocks while some other requires a low temperature condition (see Table A3 in the appendix). Likewise, CGDS process for composites-based nanomaterial coating is also performed under the same deposition conditions used for a composite mixture (Section 4.1).

The deposition of nano-scaled elements represents a singular case of the cold spray process. Very limited literature is available about the integration of CNTs or nanodiamond (ND) using this technology [81–84]. The nanosized material is typically mixed with metallic powders during a ball milling preparation step. The effective combination of the CNTs or ND into the metallic powders generally requires several hours of ball milling. Available data also provides an indication of the use of fine metals powder (see Table A5 in the appendix). Cho *et al.* used a powder particle size of 0.5-3 $\mu\text{m}$  and 20 hours of ball milling was performed to obtain the mixture of multiwall carbon nanotubes (MWCNTs) with copper [82]. This preparation enables the robust integration of the MWCNTs with the copper powder. The milling produces spherical agglomerates (with a diameter of about 20  $\mu\text{m}$ ). The exact granulometry was not reported [82]. Pialago *et al.* have performed a similar preparation but with a different ratio of CNTs and a relatively short milling time (4h). The authors used a No.400 sieve to get a final composite powder with the size of about 40 $\mu\text{m}$  [83]. Woo *et al.* reported the effects of various ball milling conditions when preparing a mixture of 10  $\mu\text{m}$  sized Al powder with nanodiamond crystals (with an individual size of 5 nm and an agglomerate with the size of 200 nm) [84]. The ND-Al particles become homogeneous in terms of morphology and size distribution with the increase

of milling time. The particles also evolve from an irregular shape towards a rounded shape with their size decrease. From the parametric studies of ND-Al and MMC powders, the correlation between the particle size, mechanical properties and milling conditions were determined [84]. Generally, the appropriate ball milling preparation can provide the suitable agglomerate size for the cold spray process that can also be used with the usual deposition conditions.

Although the direct deposition of nanopowders is possible using the cold spray technique, it requires a very low working pressure in the range of 0.1-20 kPa in a vacuum chamber [38]. A non-heated gas is also generally used during the nanopowder depositions. The available data further explains the deposition conditions including the suitable transverse velocity of the nozzle (~ in the order of few mm/s), a short standoff distance (~ 3-9 mm), and a specific nozzle throat with a cross section of approximately 2.5 x 0.2 mm. These deposition conditions enable to produce nanoporous coating for dye-sensitized solar cell (DSSC) applications. However, there can be a variance of these parameters depending on the requirement of the coating function. Recommendations for process parameters can be found in [41] which explains the sensitivity of the coating thickness to the standoff distance (SoD). Moreover, it may also require to have a very short SoD of few hundred micrometers when producing a very thin layer of coating [41].

Some other studies have investigated to fabricate nano-architected materials using the usual cold spray powders (i.e. micron sized powders) [65,66,86,87]. "Nano-architected" stands for a structure that contains nano size geometrical features. The nanoporous TiO<sub>2</sub> commonly used in photovoltaic or photocatalytic application is a typical example in the literature. Prior to the deposition, the nanopowders are mixed with a removable PEG solution and are prepared using a rotary evaporation method to produce the primary TiO<sub>2</sub>-PEG composite powder [86], and then transformed into small particles (0.5-3 $\mu$ m) by crushing operation. A vacuum deposition is then performed with the crushed particles. The PEG phase is then removed using a post annealing treatment to form the required nanoporous structure within the coating [66,86]. Such coating method provides a higher density of nanopores than that of a porous coating obtained using a direct deposition of primary TiO<sub>2</sub> nanopowder, under the same deposition conditions. Therefore, the nanopores generated with the composite powders provide an improved photocatalytic activity and a thicker coating of up to several  $\mu$ m thickness in comparison with a few  $\mu$ m thickness obtained from a direct nanopowder deposition [86]. In [35,87], a direct deposition of nanoporous powder is suggested without any major modification in terms of deposition parameters. To obtain the nanoporous powder, the PEG phase was removed after a rotary evaporation and it was treated using both chemical procedure and sintering before the crushing step [35, 87]. These additional steps enable to improve the consolidation mechanism between the nanoparticles within the porous structure. It also provides bimodal-sized nanopores which contribute for an improved photovoltaic efficiency compared to conventional unimodal distributed nanoporosity [87]. However, the overall energy conversion efficiency of a dye sensitive solar cell (DSSC) produced using the later method (the direct deposition of nanoporous powder) is lower than that of obtained from former one (powder with the PEG deposition and the post annealing removal) [86].

### 4.3 Hybrid coating/substrate deposition

Among this category, the case of ceramic/metal combination mainly depends on the knowledges acquired through the developments of the cold spray process. The usual working conditions identified for the metal/metal combinations are suitable for the deposition of a

ceramic powder onto various metallic substrates (Table A6 in the appendix). A gas pressure of 1-3 MPa and a temperature between 500-800°C enables the WC-Co or NiO-Al<sub>2</sub>O<sub>3</sub> coatings. A low pressure lying in between 0.6-0.8 MPa and a temperature of about 280°C were applied to deposit SiC particles onto an Inconel substrate (Table A6).

Inversely, a metal/ceramic combination requires extra care to facilitate a good adhesion. The deposition of spherical aluminium particles onto a lead zirconate titanate (LZT) substrate was found to be difficult due to the brittle behaviour of the LZT [19]. The fracture is occurred under the collision surface and submicronic fragments are ejected from the LZT surface. As evidenced by a grain pull-out phenomenon due to an intergranular crack formation, this event can be controlled by increasing the velocity of the particle so that the particles' impact becomes favourable to adhesive and resistant to erosion [19]. Thereby, King *et al.* have presented three solutions to obtain adhesive condition by; (1) decreasing the particle size, (2) increasing the gas temperature, or (3) increasing the gas pressure. The reduction of the particle size is also beneficial in terms of providing momentum reduction which minimizes the surface deterioration. Note that a gas temperature increase may become detrimental due to a delamination which results from the thermal stresses while the substrate is subjected to the gas stream and reaches a certain threshold temperature. Optimal spray parameters are required for the deposition of aluminium powders without causing harmful structural defects [19]. King *et al.* used a mean particle diameter of 15µm as the lowest powder size. Zhang *et al.* performed the deposition of aluminium powder onto a glass substrate with nearly round shape particles whose characteristic size varies in between 15-75 µm. Their results indicate a poor coating capability despite the observation of some anchored particles [17]. Kim *et al.* considered using fine and angular copper particles with a size of 0.5-1.5µm to produce a coating of up to 300µm thickness. Their spraying conditions include a low working pressure (0.6 MPa) and a temperature of 280°C. Adhesions of single particles and aggregated fine particles were observed, the latter revealed more apparent anchoring effect [18]. Hence, the natural agglomeration of fine particles within the gas flow seems to facilitate the adhesion, probably due to better penetration of the multi-faceted agglomerates onto the substrate.

For polymer metallization (deposition of metals on polymers), the experimental spraying conditions are rather broad. High thermal sensitivity of polymers has led to various possible depositions (Table A6 in the appendix). Those depositions can be classified into the following general conditions:

- Using the usual pressure, low temperature, with usual CGDS powder sizes
- Using a very low pressure, room temperature, with nano size powders

A considerable amount of the works on the polymer metallization using the cold spray technique relies on the expertise learned from the deposition of metal/metal combinations. Deposition is generally performed with the same conditions of the powder granulometry and the propellant gas pressure. Generally, the particle size varies in between 5-50 µm and a gas pressure of 1-3 MPa suits for the deposition. To minimize the thermal effect on the polymer substrate due to the gas flow, the preheating temperature of the propellant gas is set as approximately below 500°C. The expansion of the gas in the nozzle also reduces the temperature at the nozzle exit. Although the particles adhere onto the substrate, the deposit growth may fail due to the low velocity of particles and the low temperature which are well below the critical velocity to produce the metal/metal contact [20,21]. Hence, soft metals with a low melting temperature such as tin, zinc and aluminium are normally suitable for the CGDS polymer metallization [25,26]. Some other studies suggest the deposition of an intermediate metallic layer to promote the growth of the coating thickness on a polymer substrate. A successful deposition of a thick copper coating of up to 800 µm was produced on a PVC

substrate using an intermediate copper or tin layer, and the deposition of tin layer was particularly obtained at a low temperature and a low pressure condition [20,21]. To facilitate the coating formation, spherical powders were used to obtain the intermediate bonding layer while the top coating was made of dendritic particles. The metallization of polymer matrix composite (PMC) substrates is also possible without either erosion or damage. For example, carbon or glass fibre reinforced composites with brittle nature was coated using soft metals as reported in [20,21,25,26]. Among various metals (Al, Sn, Cu, Pb, Zn and SS316L), a good deposition capability was demonstrated for a tin (Sn) powder onto an epoxy or glass fibre reinforced composite, and for an aluminium powder onto a carbon fibre reinforced PEEK [20,21,25,26]. A low impact energy of a few  $\mu\text{J}$  is recommended to avoid the degradation of polymer during the coating process [25]. Chun *et al.* have used tin nanopowders for the metallization of some polymer substrates [88]. The deposition is performed under a vacuum condition at room temperature. It was indicated that the nanomanufacturing method was performed using a nozzle with a narrow exit with a size of 300  $\mu\text{m}$ .

The polymer/metal hybridization also represents a particular case in the literature. Very few papers have been published in this area [29,40]. In contrast with metals and ceramics, the thermoset polymers are very light and very soft materials. According to experimental investigations, the cold spray deposition of polymer powders is tricky. During the deposition, the interfacial shearing combined with the dragging action caused by the transverse wall jet flow on the substrate removes the polymer layer that was already formed during a prior impact [29]. In order to overcome this issue, a nozzle that is long enough to generate shock waves is connected to a diffuser at the exit section [29]. The shock waves provide beneficial effects for the deposition of polymer particles. That is, inside the diverging part of the long nozzle, the gas compression is induced by the shock wave and consequently it heats the particles and promotes a good deposition. At the nozzle exit, the particle velocity is reduced thus it reduces the interfacial shearing during the collision onto a previously deposited layer. Excellent quality deposition was obtained with the gas pressure and temperature of 0.5 MPa and 275  $^{\circ}\text{C}$ , respectively [29]. In [40], the successful adhesion was achieved without requiring either substrate preheating or a deposition of an intermediate metallic layer as suggested earlier.

## **5. Substrate treatment and its contributions**

The conditions of the substrate surface, in terms of topology and temperature, affect the adhesion of cold sprayed particles. At present, the papers published on this subject can be organized into three major categories including the effects of (1) surface roughness, (2) substrate heating and (3) surface texturing. The subsections 5.1-5.3 report various findings for each one of these effects on the adhesive behaviour.

### **5.1 Effects of surface roughening on the adhesive behaviour**

In cold spraying, a well prepared surface, free of contaminants and oxides is believed to promote a good bonding. Prior to the deposition, preparation of the substrate surface is generally recommended. Degreasing and cleaning steps are normally used for glass and polymer substrates. For metals, the typical practice consists of sandblasting or grit blasting or grinding and/or polishing. Sandblasting and grit blasting are generally suggested to remove the surface oxide but also to provide a roughened fresh surface, considered as an activated surface. The “activated surface” means that the surface is conducive to the particle adhesion unlike the ‘non-activated’ one that facilitates the particles to rebound. These terms were employed for metallic substrates and the activation factor is related to the surface roughness. Some studies found a

positive effect of the roughening on the bond formation [89–92] while some other analysis showed the opposite effect [76,92]. Therefore, it brings the need for a comprehensive discussion about the roughness effect on the adhesion. The best surface preparation differs for various powder/substrate combinations. For instance, Wayne *et al.* investigated the effect of roughness on the adhesion of titanium particles onto a sapphire substrate [93]. An improved adhesion with a coating thickness of 250  $\mu\text{m}$  was obtained on the polished substrate that had a roughness of lower than 3 nm in comparison with a submicron roughness for a grounded surface which rather produces a non-uniform coating of 150  $\mu\text{m}$ . Some other findings for various metal combinations are also consistent with this tendency [89–92]. Although polishing and grinding produce a deposition with comparable bonding strength, grit blasted surface mitigate the strength (Table 2). Yin *et al.* explain the decrease in bonding strength (of 24%) as a consequence of a discontinuous contact at the particle/substrate interface for a grit blasted surface [90]. However, such defective bonding is only observed for the particles' sizes close to the sizes of cavities that were produced during the grit blasting whereas the powder feedstock essentially requires containing larger powder particles than that of the cavities. Hussain *et al.* have noticed a significant decrease of the bonding strength between a polished surface ( $R_a=0.05\mu\text{m}$ ) and a grit blasted one with a roughness of 3.9 $\mu\text{m}$  [91]. According to their experimental observations, the roughness hinders the interfacial jetting during the impact and consequently it prevents the oxides removal [91]. Hence, the automatic surface cleaning during the process is disturbed and it eventually obstructs the formation of a metallurgical bond [91]. Note that the negative effect of the roughness on the bonding strength is not a paradigm, although agreements between some studies were found (Table 2). In contrast, many other studies suggest that the roughness may be beneficial to the adhesion [76,92,94]. Richer *et al.* have found that a coarse grit blasting improves the deposition efficiency of an Al-Mg powder on a Mg substrate [76]. Wu *et al.* have identified the favourable conditions of the substrate roughening. At low impact velocities, Wu *et al.* identified a flawless deposition of an Al-Si powder onto a grit blasted mild steel substrate while a polished substrate was difficult to coat under the same spraying conditions [92]. However, the bonding strength was comparable for the onset of the successful depositions in both cases. With an increase of the impact velocity, there is a range of roughness which decreases the bonding strength due to an incomplete contact within the micro-asperities whereas a polished surface facilitates a continuous contact between the particle and the substrate. The negative effect of the roughness decreases and eventually disappears when the impact velocity is high enough to deform the particles onto the roughened surface of the substrate providing an improved mechanical interlocking and thus, it forms a continuously bonded interface. These various results preclude a general rule for surface roughening for the cold spray process. The recommendation of sandblasting or grit blasting is rather useful to remove the oxides from the metal surfaces. Moreover, this method is currently being followed for the surface preparation.

## 5.2 Effects of substrate heating on the adhesive behaviour

Some research studies were focused on the influence of substrate heating on deposition. Legoux *et al.* investigated the deposition of hard, medium and soft particles using Al, Zn, and Sn powder feedstocks. A grit blasted carbon-steel substrate was preheated to 350°C and an infrared high-speed camera (ThermaCAM SC3000) was used to measure the surface temperature during the deposition [95]. It was shown that the deposition efficiency increases for the aluminium, decreases for the zinc and remains low without any changes for the tin. Based on microstructural observations, the increase in DE for the Al particles seems to be related to the particle deformation while the adhesion of Zn particles suffers from an oxidation although elongation and strong deformation of those particles were observed. For the tin, the effect of the substrate

heating was not conclusive since the gas conditions enabled a velocity which was favourable for erosion. Fukumoto *et al.* performed deposition of copper on a SS and an Al substrates both had 0.3  $\mu\text{m}$  roughness. The propellant gas was not heated in their study to avoid the additional thermal effect caused by the gas itself. Increased substrate temperatures were identified as conducive to improve the DE in those experiments. Using a gas pressure of 5bar and a particle mean size of 5 $\mu\text{m}$ , a DE of up to 80% was achieved with a substrate temperature of 600°C, while a substrate at room temperature provides a DE of lower than 20% under the same experimental conditions [96]. Although, low number of crater formation was observed with substrate heating, the underlying mechanism in the improvement of the deposition was not further clarified. Yu *et al.* suggested some improvements in the deposition with the substrate heating using a numerical simulation of both particles and substrate behaviours [97]. The thermomechanical softening of the substrate allows embedding the particles further into the substrate, which was interpreted as an interlocking mechanism that governs the bonding. A virtual test of a Cu/Cu combination also revealed that the contact area remained nearly unchanged for a substrate temperature varies of 100-600 °C. According to the authors, such situation limits the role of mechanical interlocking. However, the literature agreed that the thermomechanical softening due to substrate heating promotes the adhesion during the cold spray process [97–101]. In case of a deposition onto a hard substrate such as Al<sub>2</sub>O<sub>3</sub> with Cu particles [94], substrate heating is believed to enable an activation effect. By increasing the substrate temperature, the evaporation and decomposition of adsorbate occur on the free surface of Al<sub>2</sub>O<sub>3</sub> and then a direct metal/ceramic contact happens at the Cu/Al<sub>2</sub>O<sub>3</sub> interface during the cold spray deposition [94].

### 5.3 Effects of surface texturing on the adhesive behaviour

A recent novel type of surface preparation arises from the laser technology known as surface texturing. A high fidelity pattern on a surface is produced using a sophisticated equipment with a high energy laser impulse. Repetition of the specific laser ablation procedure using an automated scanning method is performed to obtain various patterns. The laser treatment generates a textured surface whose characteristics vary with the diameter and depth of the holes, the inter-hole distance and the orientation of the holes, which are tailored by the laser impulse. The laser texturing provides a regular surface topography with an optimizable pattern in terms of the shape and size. Kromer *et al.* have found an improvement in the adhesive behaviour using a laser texturing method [102,103]. Fig. 10 shows the cases of a weakly textured surface (Texture 1) and a highly textured surface (Texture 2). Cold spraying tests were performed on each textured surface and compared with a coating performed on a grit blasted surface with a roughness of 2.7 $\mu\text{m}$ . The bonding strength increases two fold or even more, when using those textured surfaces (Fig. 11). The texturing method improves the mechanical anchoring of the particles on the substrate. The deposited particles fill the holes of the pattern. This evidence shows a convincing solution for an improvement of the bonding strength of cold spray coatings provided that the substrate is sensitive to the laser texturing method.

### 6. Prospective improvements based on the powder features

Selection of the powder features plays a major role in the deposit formation. In the cold spray literature, analyses have been focused on the effects of some of these features regardless of the material of the powder feedstock. To date, the kinematic effect of the particle size is known. However, the suitable particle size to reach the critical velocity and consequently to cause a successful adhesion is also a main subject of various research studies. For this purpose,

researchers used various experimental measurement techniques and numerical models as mentioned in Section 2.2. Nevertheless, the specific features of the powder such as the (1) particles' temperature, (2) morphology, and (3) inner architecture have their own significance in the bond formation. The details of these specific features are given in the sub sections 6.1-6.3.

### 6.1 Effect of temperature of the powder

Although the particle velocity prior to impact is a parameter that mainly governs the deposition, the particle temperature can also promote the adhesion. Various empirical models have shown that the critical velocity of adhesion ( $V_{cr}$ ) decreases with the increase in the particles' temperature [104–106].  $V_{cr}$  is found to be dependent of particles' temperature according to the following generic rule  $\sqrt{1 - T_p/T_m}$  that gives a coefficient with a numerical value of lower than one; where  $T_p$  and  $T_m$  are the particles' temperature prior to the impact and the melting temperature of the particles, respectively. Schmidt *et al.* claimed that the deposition window defined in terms of  $V_{cr}$  based on  $T_p$  has a low temperature limit and below this temperature the material may follow a brittle behaviour, and above which the material becomes ductile and it enhances the bonding [104]. That is, the thermomechanical softening of the particles due to  $T_p$  is interpreted as a factor that facilitates the bonding. It is also believed to increase the area of metallurgically bonded interface during the cold spray deposition [105].

Generally, there are two distinct methods to heat the particles either via setting the inlet gas at a high temperature or using preheated particles. But at present, a reliable quantification of the particles' temperature in cold spraying suffers from real complexities due to technical limitations. Particularly, due to the small size of the particles used in cold spraying, experimental measurement of the particles' temperature is difficult to be obtained. Using numerical models including the heat transfer effect over the particles' surface is an alternative way to compute the particles' temperature within the gas flow but the reliability of this assessment has not clearly been discussed. Nevertheless, some analysis focused on the change in mechanical properties due to a long preheating step of the powder feedstock [107,108]. During the preheating step, it involves a decrease in the hardness of the particles due to an annealing effect and a stress relaxation which increase the DE [107,108]. The same annealing conditions in a vacuum provides a high DE than that of an annealing treatment performed in a non-vacuum environment which causes oxidation [108]. Eventually, the oxide layer obstructs the formation of a metallurgical bonding. Thus the oxide layer has to be broken and ejected during the deposition to obtain a successful adhesion. Thereby, the oxygen content in the annealed powders increases the critical velocity of adhesion. Experimental findings show that the required  $V_{cr}$  can substantially increase due to the surface oxidation [104,109–111].

### 6.2 Effect of morphology of the powder

The cold spray process is not exclusively used with spherical powders albeit they have always been considered as the conventional powders. The nature of the powder feedstock also includes the case of irregular morphologies such as angular and dendritic shapes. Generally, spherical powders are produced by atomization whereas angular powders are produced by cryomilling. Dendritic powders are obtained using an electrolytic production method. Some studies showed a substantial gain in the DE using the irregular particles. Unlike the spherical powders, they give higher in-flight velocity for the same deposition conditions and similar granulometry [107,112]. Similar deposition conditions with the use of similar granulometry of the powders confirm the capability of irregular particles to reach the highest possible velocities [113]. The

kinematic gain of irregular powders is attributed to a higher drag coefficient due to a rapid boundary layer separation over the particles' surface. The higher drag coefficient generates a negative pressure gradient, and consequently a large drag force that allows the particles to reach high velocities [114,115]. Therefore, the irregular morphology improves the deposition efficiency, decreases the porosity within the deposit. Thus it can also enable the increase in the hardness of the coating [112,114].

In literature of cold spraying, comparison between dendritic powders and spherical powders were also investigated. Deposition of spherical particles fails whereas dendritic particles produce dense coating with a high DE [116–118]. Irregular morphology enables the particles to reach high impact velocities and better heating. In addition, the free space between the dendrites acts as a porous-like structure that confers lower elastic modulus and yield strength [116]. Thus, dendritic powders have lower critical velocity than that of spherical powders. Therefore, high quality coatings can be manufactured at low temperatures using dendritic powders with a DE of up to 80% [117]. With this capability, dendritic powders have been used to get successful deposition on the thermally sensitive substrates such as polymers, or to improve the DE when using a low pressure cold spray (LPCS) deposition [21,118–121]. The deposition of dendritic powders on a polymer substrate is also found to limit the erosion. Moreover, LPCS brings innovative contributions such as developments of hybrid deposit/substrate combinations [20,25,29], in-situ restoration using a portable LPCS system [122], deposition using thermally sensitive materials [25,29]. Furthermore, one can produce deposits with metals and MMCs using spherical powders when the deposition using LPCS method is less efficient for such materials due to the kinematic limitation of the propellant gas.

### 6.3 Effect of the inner architecture of the powder

New term "powder architecture" can be suggested to note a distinction with the term "powder morphology" which generally refers to the shape of the powder, and particularly the outer shape. New powder types are rather characterized by their specific inner features. In the literature for cold spraying, the cases of porous powders and cladded powders can be identified as type of powder architectures for which a very limited literature is available. It includes the following distinct types: porous architecture (sponge powders) and core-coated architecture (cladded powders: i.e. the core made of a particle is cladded by a thin coating made of a distinct material).

Wong *et al.* depicted various depositions using powders with sponge architecture [112]. In contrast to spherical powders, angular powders and sponge powders can reach higher impact velocities as they have higher drag coefficients under the same deposition conditions [112]. Thus, a good adhesion is obtained for both angular and sponge powders and the DE is also similar and higher than that of obtained for the spherical powders using similar deposition conditions. Both sponge and angular powders exhibit similar coating quality except for the hardness and the porosity of the coating. Although their primary hardness is the lowest for sponge powders, they generate the highest hardness within the coating. Indeed, the hardness ratio ( $HV_{\text{coating}}/HV_{\text{powders}}$ ) for sponge powders can reach 2.1-2.65 in comparison with (1.5-1.95) and (1.35-1.6) obtained for angular powders and spherical powders, respectively (the hardness of the primary sponge, angular and spherical powders are respectively ~92HV, ~120HV and ~142HV). Regarding the porosity, the porous architecture of the sponge powders facilitates the formation of residual pores within the coating. The amount of porosity is the highest compared to the case of angular and spherical powders. However, in some other studies, the porosity of primary porous powders provides an advantage in terms of the improvement of energy conversion efficiency of DSSCs [86] as reported in Section 4.2. The deposition of the porous

powders produces bimodal-sized nanopores that enable to increase the photovoltage of DSSCs [87].

Core-coated architecture has been investigated as an alternative technique to deposit non-ductile materials such as ceramics, oxides and diamond. Such powders are known to be hard and brittle. Due to the high velocity impact during the cold spray process, they suffer from crack formation which affects the structural integrity of the coating. The literature presents several successful depositions using a mixture of these powders with metallic powders. The metal phase which is ductile, acts as a binder and also experiences plastic deformation. Thus it facilitates the deposit formation and improves the structural integrity of the coating by absorbing the impact energy via the plastic deformation. To produce the same effect, the use of cladded powders was suggested in [67,68]. Diamond powders were precoated by two thin layers (~2-5 $\mu\text{m}$ ) with Ni and Cu as the inner and outer layers, respectively. The Ni clad was used as an intermediate layer to bond the diamond to Cu. The cold spray deposition of the cladded diamond powders onto an Al substrate produced a successful coating [68]. However, the clad layer was not sufficiently thick to completely absorb the kinetic energy of the collision. Hence, the diamond core was fragmented due to high stresses during the collision on the substrate. Nonetheless, the fabrication of a thick coating exceeding 5mm was demonstrated [67].

## 7. Conclusions and future perspectives

Since it discovered in the early 19<sup>th</sup> century, the cold spray method has been improved over decades and integrated with a major innovation step of using a De Laval nozzle. With the help of significant research works including the fundamental developments at the Institute of Theoretical and Applied Mechanics of the Russian Academy of Science, the cold spray manufacturing method has evolved as an innovative cold additive material processing technique. Various phenomena during the deposit formation and the growth of the coating have been characterized by many researchers. Several distinct mechanisms were identified and it revealed the enormous capabilities of the cold spray process. Various technological deposits have been obtained and in this context ample experimental data are available in the literature. In this review, the cold spray method is categorized using a taxonomy based on both the deposition procedure and innovative material perspectives. Thus, a comprehensive review of deposition procedures includes the following classifications: baseline working conditions for the cold spray process, specific processing conditions including the deposition of nanotechnological deposits, deposition of composites-based deposits, and hybrid coating/substrate deposition. Available data are gathered to constitute an experimental database with a wide overview of the required processing conditions for the cold spray additive manufacturing.

Deposition of metals has led to typical experimental conditions of cold spraying, including gas pressure and temperature of up to 5MPa and 800 °C, respectively, which is mainly suitable for the micron size powders. He, N<sub>2</sub> or air can be used as the propellant gas for the deposition among which He is the most efficient one due to its high specific gas constant and low molecular weight. Small size particles are deposited using a vacuum chamber while the propellant gas is set to sub-atmospheric pressures without preheating. Those conditions are specially recommended for fine powders (20nm-5 $\mu\text{m}$ ).

The baseline working conditions of cold spraying are often used to deposit the composite powders. The composite powder deposition can be achieved using two distinct methods: using a single point injection of a premixed powder feedstock in the nozzle or using a multi-point

injection for each powder feedstock at different zones of the nozzle. With the first method, deposition can be difficult for dissimilar powders mixture such as metal/ceramic combinations due to differences in both mechanical and thermal properties. Moreover, an agglomerated mixture prepared by a strong mechanical mixing and grinding was used to facilitate the adhesion. With the second method, it is possible to simultaneously reach the optimal adhesive conditions for each powder component. In this method, the powders become mixed inside the nozzle to form the deposit of the composite on the substrate. This deposition method recommends that easily processable powders (requiring low temperature for successful coating) are injected in the supersonic region of the nozzle, and the difficult one (requiring higher temperature) in or near the subsonic region of the nozzle.

The literature for cold spraying also shows the substantial efforts in manufacturing the hybrid deposit/substrate components. The typical cold spray conditions of metal pairs are used for the ceramic/metal combination. For other hybrid combinations, such as oxide/ceramic, oxide/polymer, metal/polymer, metal/PMCs, polymer/metal and metal/ceramic; the deposition using a low pressure and a low temperature is recommended. When using nanoparticles, vacuum deposition is recommended while the propellant gas is set to a sub-atmospheric pressure which is suitable to achieve a deposit/substrate hybridization without thermal damage of the substrate.

The review on the surface conditions for the substrate is classified into three main categories based on their contributions: (1) surface roughening, (2) substrate temperature and (3) surface texture. For metals, the typical practice of surface preparation consists of sandblasting or grit blasting or grinding and/or polishing. Various effects of the substrate roughness on the adhesion and bonding strength preclude a general rule for surface roughening in cold spraying. As used in typical surface preparation, sandblasting or grit blasting is rather recommended to remove the oxides from the metal surfaces. Prior to deposition, the substrate surface can also be textured using a laser technology to provide a regular pattern of micro holes which are filled with the particles during their collisions onto the substrate. This method creates regular bond and improves the bonding strength. The other surface treatment is the substrate heating method during the deposition. The literature shows that the thermomechanical softening due to substrate heating promotes the adhesion.

The literature of cold spraying also includes the consideration of the following specific features of the powders: the particles' temperature, the powders' morphology, and the powders' inner architecture. Heating of the particles modifies the mechanical properties of the powders and thus it facilitates the bonding during the deposition. It is believed that the critical velocity of adhesion decreases with the heating of the particles. Regarding particles' morphology, comparative studies of various shapes (spherical, angular and dendritic) were performed. Irregular morphology (e.g. angular or dendritic) improves the deposition efficiency, decreases the porosity within the deposit, and thus it increases the hardness of the coating. Finally, effects of inner architecture of the powder were shown in this review. Porous powders reach the highest possible impact velocities because of their high drag coefficient. A good adhesion and a high DE are obtained for porous powders. Cladded powders made of a ceramic core (or another hard material) and a thin ductile coating (using a soft material), also produce a successful deposit when the ductile coating acts as a binder during the deposit formation.

Although the CGDS process has gained numerous experimental benefits till to date, the efficiency of the new emerging applications relies on (1) prediction of the process behaviour including the thermal kinetics of the particle within the gas flow, (2) optimization of deposition

efficiency and (3) prediction of structural changes during the deposit formation that governs the final properties of the deposit. Together, such future works could open new avenues to a wide range of efficient CGDS methods.

ACCEPTED MANUSCRIPT

## References

- [1] E. Irissou, J.-G. Legoux, A.N. Ryabinin, B. Jodoin, C. Moreau, Review on Cold Spray Process and Technology: Part I—Intellectual Property, *J. Therm. Spray Technol.* 17 (2008) 495–516. doi:10.1007/s11666-008-9203-3.
- [2] Krömer, Werner, Overview of the global Thermal Spray Market and Trends in Europe, *Weld. Cut.* (2012) 377.
- [3] T.H. Van Steenkiste, J.R. Smith, R.E. Teets, Aluminum coatings via kinetic spray with relatively large powder particles, *Surf. Coat. Technol.* 154 (2002) 237–252. doi:10.1016/S0257-8972(02)00018-X.
- [4] H. Assadi, F. Gärtner, T. Stoltenhoff, H. Kreye, Bonding mechanism in cold gas spraying, *Acta Mater.* 51 (2003) 4379–4394. doi:10.1016/S1359-6454(03)00274-X.
- [5] M. Grujicic, C.. Zhao, C. Tong, W.. DeRosset, D. Helfritsch, Analysis of the impact velocity of powder particles in the cold-gas dynamic-spray process, *Mater. Sci. Eng. A.* 368 (2004) 222–230. doi:10.1016/j.msea.2003.10.312.
- [6] H.Y. Lee, Y.H. Yu, Y.C. Lee, Y.P. Hong, K.H. Ko, Interfacial studies between cold-sprayed WO<sub>3</sub>, Y<sub>2</sub>O<sub>3</sub> films and Si substrate, *Appl. Surf. Sci.* 227 (2004) 244–249. doi:10.1016/j.apsusc.2003.11.073.
- [7] Y. Kim, S. Yang, J.-W. Lee, J.-O. Choi, S.-H. Ahn, C.S. Lee, Photovoltaic Characteristics of a Dye-Sensitized Solar Cell (DSSC) Fabricated by a Nano-Particle Deposition System (NPDS), *Mater. Trans.* 54 (2013) 2064–2068. doi:10.2320/matertrans.M2013220.
- [8] H.Y. Lee, Y.H. Yu, Y.C. Lee, Y.P. Hong, K.H. Ko, Thin Film Coatings of WO<sub>3</sub> by Cold Gas Dynamic Spray: A Technical Note, *J. Therm. Spray Technol.* 14 (2005) 183–186. doi:10.1361/105996304523791.
- [9] D.-M. Chun, S.-H. Ahn, Deposition mechanism of dry sprayed ceramic particles at room temperature using a nano-particle deposition system, *Acta Mater.* 59 (2011) 2693–2703. doi:10.1016/j.actamat.2011.01.007.
- [10] S.-Q. Fan, C.-J. Li, G.-J. Yang, L.-Z. Zhang, J.-C. Gao, Y.-X. Xi, Fabrication of Nano-TiO<sub>2</sub> Coating for Dye-Sensitized Solar Cell by Vacuum Cold Spraying at Room Temperature, *J. Therm. Spray Technol.* 16 (2007) 893–897. doi:10.1007/s11666-007-9090-z.
- [11] M. Yamada, H. Isago, H. Nakano, M. Fukumoto, Cold Spraying of TiO<sub>2</sub> Photocatalyst Coating With Nitrogen Process Gas, *J. Therm. Spray Technol.* 19 (2010) 1218–1223. doi:10.1007/s11666-010-9520-1.
- [12] S.-Q. Fan, G.-J. Yang, C.-J. Li, G.-J. Liu, C.-X. Li, L.-Z. Zhang, Characterization of Microstructure of Nano-TiO<sub>2</sub> Coating Deposited by Vacuum Cold Spraying, *J. Therm. Spray Technol.* 15 (2006) 513–517. doi:10.1361/105996306X146901.
- [13] D. Rafaja, T. Schucknecht, V. Klemm, A. Paul, H. Berek, Microstructural characterisation of titanium coatings deposited using cold gas spraying on Al<sub>2</sub>O<sub>3</sub> substrates, *Surf. Coat. Technol.* 203 (2009) 3206–3213. doi:10.1016/j.surfcoat.2009.03.054.
- [14] Amadeu Concustell, Features of Coatings Built-Up by Cold Gas Spray, (2015).
- [15] D. Giraud, Étude des composantes mécanique et métallurgique dans la liaison revêtement-substrat obtenue par projection dynamique par gaz froid pour les systèmes «Aluminium/Polyamide6,6» et «Titane/TA6V», Thèse de doctorat, ENSMP MAT. Centre des matériaux, 2014.
- [16] M. Grujicic, J.R. Saylor, D.E. Beasley, W.S. DeRosset, D. Helfritsch, Computational analysis of the interfacial bonding between feed-powder particles and the substrate in the cold-gas dynamic-spray process, *Appl. Surf. Sci.* 219 (2003) 211–227. doi:10.1016/S0169-4332(03)00643-3.
- [17] D. Zhang, P.H. Shipway, D.G. McCartney, Cold Gas Dynamic Spraying of Aluminum: The Role of Substrate Characteristics in Deposit Formation, *J. Therm. Spray Technol.* 14 (2005) 109–116. doi:10.1361/10599630522666.

- [18] D.-Y. Kim, J.-J. Park, J.-G. Lee, D. Kim, S.J. Tark, S. Ahn, J.H. Yun, J. Gwak, K.H. Yoon, S. Chandra, S.S. Yoon, Cold Spray Deposition of Copper Electrodes on Silicon and Glass Substrates, *J. Therm. Spray Technol.* 22 (2013) 1092–1102. doi:10.1007/s11666-013-9953-4.
- [19] P.C. King, S. Zahiri, M. Jahedi, J. Friend, Aluminium coating of lead zirconate titanate—A study of cold spray variables, *Surf. Coat. Technol.* 205 (2010) 2016–2022. doi:10.1016/j.surfcoat.2010.08.084.
- [20] A. Ganesan, M. Yamada, M. Fukumoto, Cold Spray Coating Deposition Mechanism on the Thermoplastic and Thermosetting Polymer Substrates, *J. Therm. Spray Technol.* 22 (2013) 1275–1282. doi:10.1007/s11666-013-9984-x.
- [21] A. Ganesan, J. Affi, M. Yamada, M. Fukumoto, Bonding behavior studies of cold sprayed copper coating on the PVC polymer substrate, *Surf. Coat. Technol.* 207 (2012) 262–269. doi:10.1016/j.surfcoat.2012.06.086.
- [22] I. Burlacov, J. Jirkovský, L. Kavan, R. Ballhorn, R.B. Heimann, Cold gas dynamic spraying (CGDS) of TiO<sub>2</sub> (anatase) powders onto poly(sulfone) substrates: Microstructural characterisation and photocatalytic efficiency, *J. Photochem. Photobiol. Chem.* 187 (2007) 285–292. doi:10.1016/j.jphotochem.2006.10.023.
- [23] D. Seo, M. Sayar, K. Ogawa, SiO<sub>2</sub> and MoSi<sub>2</sub> formation on Inconel 625 surface via SiC coating deposited by cold spray, *Surf. Coat. Technol.* 206 (2012) 2851–2858. doi:10.1016/j.surfcoat.2011.12.010.
- [24] T. Hussain, D.G. McCartney, P.H. Shipway, Bonding between aluminium and copper in cold spraying: story of asymmetry, *Mater. Sci. Technol.* 28 (2012) 1371–1378. doi:10.1179/1743284712Y.0000000051.
- [25] R. Lupoi, W. O’Neill, Deposition of metallic coatings on polymer surfaces using cold spray, *Surf. Coat. Technol.* 205 (2010) 2167–2173. doi:10.1016/j.surfcoat.2010.08.128.
- [26] X.L. Zhou, A.F. Chen, J.C. Liu, X.K. Wu, J.S. Zhang, Preparation of metallic coatings on polymer matrix composites by cold spray, *Surf. Coat. Technol.* 206 (2011) 132–136. doi:10.1016/j.surfcoat.2011.07.005.
- [27] F. Robitaille, M. Yandouzi, S. Hind, B. Jodoin, Metallic coating of aerospace carbon/epoxy composites by the pulsed gas dynamic spraying process, *Surf. Coat. Technol.* 203 (2009) 2954–2960. doi:10.1016/j.surfcoat.2009.03.011.
- [28] P.C. King, A.J. Poole, S. Horne, R. de Nys, S. Gulizia, M.Z. Jahedi, Embedment of copper particles into polymers by cold spray, *Surf. Coat. Technol.* 216 (2013) 60–67. doi:10.1016/j.surfcoat.2012.11.023.
- [29] A.S. Alhulaifi, G.A. Buck, W.J. Arbegast, Numerical and Experimental Investigation of Cold Spray Gas Dynamic Effects for Polymer Coating, *J. Therm. Spray Technol.* 21 (2012) 852–862. doi:10.1007/s11666-012-9743-4.
- [30] V.K. Champagne, D. Helfritsch, P. Leyman, S. Grendahl, B. Klotz, Interface Material Mixing Formed by the Deposition of Copper on Aluminum by Means of the Cold Spray Process, *J. Therm. Spray Technol.* 14 (2005) 330–334. doi:10.1361/105996305X59332.
- [31] K.H. Ko, J.O. Choi, H. Lee, Intermixing and interfacial morphology of cold-sprayed Al coatings on steel, *Mater. Lett.* 136 (2014) 45–47. doi:10.1016/j.matlet.2014.07.142.
- [32] R. Ghelichi, M. Guagliano, Coating by the Cold Spray Process: a state of the art, *Fract. Struct. Integr. O* (2009) pages 30-44. doi:10.3221/IGF-ESIS.08.03.
- [33] A. Moridi, S.M. Hassani-Gangaraj, M. Guagliano, M. Dao, Cold spray coating: review of material systems and future perspectives, *Surf. Eng.* 30 (2014) 369–395.
- [34] H. Assadi, H. Kreye, F. Gärtner, T. Klassen, Cold spraying – A materials perspective, *Acta Mater.* (n.d.). doi:10.1016/j.actamat.2016.06.034.
- [35] G.-J. Yang, C.-J. Li, K.-X. Liao, X.-L. He, S. Li, S.-Q. Fan, Influence of gas flow during vacuum cold spraying of nano-porous TiO<sub>2</sub> film by using strengthened nanostructured powder on performance of dye-sensitized solar cell, *Thin Solid Films.* 519 (2011) 4709–4713. doi:10.1016/j.tsf.2011.01.021.

- [36] D.-M. Chun, C.-S. Kim, J.-O. Choi, G.-Y. Lee, C.S. Lee, S.-H. Ahn, Multilayer deposition of ceramic and metal at room temperature using nanoparticle deposition system (NPDS) and planarization process, *Int. J. Adv. Manuf. Technol.* 72 (2014) 41–46. doi:10.1007/s00170-013-5327-9.
- [37] D.M. Chun, M.H. Kim, J.C. Lee, S.H. Ahn, TiO<sub>2</sub> coating on metal and polymer substrates by nano-particle deposition system (NPDS), *CIRP Ann. - Manuf. Technol.* 57 (2008) 551–554. doi:10.1016/j.cirp.2008.03.111.
- [38] D.-M. Chun, M.-H. Kim, J.-C. Lee, S.-H. Ahn, A Nano-particle Deposition System for Ceramic and Metal Coating at Room Temperature and Low Vacuum Conditions, *Int. J. Precis. Eng. Manuf.* 9 (2008) 51–53.
- [39] M. Gardon, A. Latorre, M. Torrell, S. Dosta, J. Fernández, J.M. Guilemany, Cold gas spray titanium coatings onto a biocompatible polymer, *Mater. Lett.* 106 (2013) 97–99. doi:10.1016/j.matlet.2013.04.115.
- [40] Y. Xu, I.M. Hutchings, Cold spray deposition of thermoplastic powder, *Surf. Coat. Technol.* 201 (2006) 3044–3050. doi:10.1016/j.surfcoat.2006.06.016.
- [41] K. Jung, W. Song, D.-M. Chun, Y.-H. Kim, J.-C. Yeo, M.-S. Kim, S.-H. Ahn, C.S. Lee, Nickel Line Patterning Using Silicon Supersonic Micronozzle Integrated with a Nanoparticle Deposition System, *Jpn. J. Appl. Phys.* 49 (2010) 05EC09. doi:10.1143/JJAP.49.05EC09.
- [42] F. Wang, D. Zhang, S. Zheng, B. Qi, Characteristic of cold sprayed catalytic coating for hydrogen production through fuel reforming, *Int. J. Hydrog. Energy.* 35 (2010) 8206–8215. doi:10.1016/j.ijhydene.2009.12.087.
- [43] M. Yandouzi, E. Sansoucy, L. Ajdelsztajn, B. Jodoin, WC-based cermet coatings produced by cold gas dynamic and pulsed gas dynamic spraying processes, *Surf. Coat. Technol.* 202 (2007) 382–390. doi:10.1016/j.surfcoat.2007.05.095.
- [44] G.-C. Ji, H.-T. Wang, X. Chen, X.-B. Bai, Z.-X. Dong, F.-G. Yang, Characterization of cold-sprayed multimodal WC-12Co coating, *Surf. Coat. Technol.* 235 (2013) 536–543. doi:10.1016/j.surfcoat.2013.08.021.
- [45] S. Dosta, M. Couto, J.M. Guilemany, Cold spray deposition of a WC-25Co cermet onto Al7075-T6 and carbon steel substrates, *Acta Mater.* 61 (2013) 643–652. doi:10.1016/j.actamat.2012.10.011.
- [46] M. Couto, S. Dosta, M. Torrell, J. Fernández, J.M. Guilemany, Cold spray deposition of WC-17 and 12Co cermets onto aluminum, *Surf. Coat. Technol.* 235 (2013) 54–61. doi:10.1016/j.surfcoat.2013.07.011.
- [47] A.S.M. Ang, C.C. Berndt, P. Cheang, Deposition effects of WC particle size on cold sprayed WC-Co coatings, *Surf. Coat. Technol.* 205 (2011) 3260–3267. doi:10.1016/j.surfcoat.2010.11.045.
- [48] S. Yin, M. Meyer, W. Li, H. Liao, R. Lupoi, Gas Flow, Particle Acceleration, and Heat Transfer in Cold Spray: A review, *J. Therm. Spray Technol.* 25 (2016) 874–896. doi:10.1007/s11666-016-0406-8.
- [49] G.A. Hughmark, Mass and heat transfer from rigid spheres, *AIChE J.* 13 (1967) 1219–1221. doi:10.1002/aic.690130638.
- [50] D.J. CARLSON, R.F. HOGLUND, Particle drag and heat transfer in rocket nozzles, *AIAA J.* 2 (1964) 1980–1984. doi:10.2514/3.2714.
- [51] Y.P. Wan, V. Prasad, G.-X. Wang, S. Sampath, J.R. Fincke, Model and Powder Particle Heating, Melting, Resolidification, and Evaporation in Plasma Spraying Processes, *J. Heat Transf.* 121 (1999) 691–699. doi:10.1115/1.2826034.
- [52] T. Schmidt, H. Assadi, F. Gärtner, H. Richter, T. Stoltenhoff, H. Kreye, T. Klassen, From Particle Acceleration to Impact and Bonding in Cold Spraying, *J. Therm. Spray Technol.* 18 (2009) 794–808. doi:10.1007/s11666-009-9357-7.
- [53] A.P. Alkhimov, V.F. Kosarev, A.N. Papyrin, A method of cold gas-dynamic deposition, *Sov. Phys. Dokl.* 35 (1990) 1047.

- [54] C.-J. Li, W.-Y. Li, Y.-Y. Wang, G.-J. Yang, H. Fukanuma, A theoretical model for prediction of deposition efficiency in cold spraying, *Thin Solid Films*. 489 (2005) 79–85. doi:10.1016/j.tsf.2005.05.002.
- [55] S.V. Klinkov, V.F. Kosarev, Measurements of Cold Spray Deposition Efficiency, *J. Therm. Spray Technol.* 15 (2006) 364–371. doi:10.1361/105996306X124365.
- [56] D.L. Gilmore, R.C. Dykhuizen, R.A. Neiser, T.J. Roemer, M.F. Smith, Particle Velocity and Deposition Efficiency in the Cold Spray Process, *J. Therm. Spray Technol.* 8 (1999) 576–582. doi:10.1361/105996399770350278.
- [57] R.N. Raelison, E. Aubignat, M.-P. Planche, S. Costil, C. Langlade, H. Liao, Low pressure cold spraying under 6 bar pressure deposition: Exploration of high deposition efficiency solutions using a mathematical modelling, *Surf. Coat. Technol.* 302 (2016) 47–55. doi:10.1016/j.surfcoat.2016.05.068.
- [58] J.-G. Legoux, E. Irissou, S. Desaulniers, J. Bobyn, B. Harvey, E. Gagnon, W. Wong, S. Yue, Characterization and Performance Evaluation of a Helium Recovery System Designed for Cold Spraying - International Metallographic Society, in: *Proc. Int. Therm. Spray Conf.*, Singapore, 2010: pp. 560–565. [http://www.asminternational.org/web/ims/resources/-/journal\\_content/56/10192/CP2010ITSC560/PUBLICATION;jsessionid=D72AA2E838A2295711464A6B97F16FCE?p\\_p\\_id=101&p\\_p\\_lifecycle=0&p\\_p\\_state=maximized&p\\_p\\_mode=view](http://www.asminternational.org/web/ims/resources/-/journal_content/56/10192/CP2010ITSC560/PUBLICATION;jsessionid=D72AA2E838A2295711464A6B97F16FCE?p_p_id=101&p_p_lifecycle=0&p_p_state=maximized&p_p_mode=view) (accessed March 27, 2016).
- [59] J. Pattison, S. Celotto, R. Morgan, M. Bray, W. O'Neill., Cold gas dynamic manufacturing: A non-thermal approach to freeform fabrication, *Int. J. Mach. Tools Manuf.* 47 (2007) 627–634. doi:10.1016/j.ijmachtools.2006.05.001.
- [60] W. Wong, E. Irissou, A.N. Ryabinin, J.-G. Legoux, S. Yue, Influence of Helium and Nitrogen Gases on the Properties of Cold Gas Dynamic Sprayed Pure Titanium Coatings, *J. Therm. Spray Technol.* 20 (2011) 213–226. doi:10.1007/s11666-010-9568-y.
- [61] S. Yin, X. Suo, H. Liao, Z. Guo, X. Wang, Significant influence of carrier gas temperature during the cold spray process, *Surf. Eng.* 30 (2014) 443–450. doi:10.1179/1743294414Y.0000000276.
- [62] S. Yin, Q. Liu, H. Liao, X. Wang, Effect of injection pressure on particle acceleration, dispersion and deposition in cold spray, *Comput. Mater. Sci.* 90 (2014) 7–15. doi:10.1016/j.commatsci.2014.03.055.
- [63] H. Assadi, T. Schmidt, H. Richter, J.-O. Kliemann, K. Binder, F. Gärtner, T. Klassen, H. Kreye, On Parameter Selection in Cold Spraying, *J. Therm. Spray Technol.* 20 (2011) 1161–1176. doi:10.1007/s11666-011-9662-9.
- [64] M. Fukumoto, H. Terada, M. Mashiko, K. Sato, M. Yamada, E. Yamaguchi, Deposition of Copper Fine Particle by Cold Spray Process, *Mater. Trans.* 50 (2009) 1482–1488. doi:10.2320/matertrans.MRA2008223.
- [65] Y.-Y. Wang, Y. Liu, C.-J. Li, G.-J. Yang, K. Kusumoto, Electrical and mechanical properties of nano-structured TiN coatings deposited by vacuum cold spray, *Vacuum*. 86 (2012) 953–959. doi:10.1016/j.vacuum.2011.06.026.
- [66] G.-J. Yang, C.-J. Li, S.-Q. Fan, Y.-Y. Wang, C.-X. Li, Influence of Annealing on Photocatalytic Performance and Adhesion of Vacuum Cold-Sprayed Nanostructured TiO<sub>2</sub> Coating, *J. Therm. Spray Technol.* 16 (2007) 873–880. doi:10.1007/s11666-007-9109-5.
- [67] S. Yin, Y. Xie, J. Cizek, E. Ekoi, T. Hussain, D. Dowling, R. Lupoi, Advanced diamond-reinforced metal matrix composites via cold spray: Properties and deposition mechanism, *Compos. Part B Eng. (n.d.)*. doi:10.1016/j.compositesb.2017.01.009.
- [68] B. Aldwell, S. Yin, K.A. McDonnell, D. Trimble, T. Hussain, R. Lupoi, A novel method for metal–diamond composite coating deposition with cold spray and formation mechanism, *Scr. Mater.* 115 (2016) 10–13. doi:10.1016/j.scriptamat.2015.12.028.
- [69] A. Sova, D. Pervushin, I. Smurov, Development of multimaterial coatings by cold spray and gas detonation spraying, *Surf. Coat. Technol.* 205 (2010) 1108–1114. doi:10.1016/j.surfcoat.2010.07.092.

- [70] A. Sova, V.F. Kosarev, A. Papyrin, I. Smurov, Effect of Ceramic Particle Velocity on Cold Spray Deposition of Metal-Ceramic Coatings, *J. Therm. Spray Technol.* 20 (2011) 285–291. doi:10.1007/s11666-010-9571-3.
- [71] S.V. Klinkov, V.F. Kosarev, A.A. Sova, I. Smurov, Deposition of multicomponent coatings by Cold Spray, *Surf. Coat. Technol.* 202 (2008) 5858–5862. doi:10.1016/j.surfcoat.2008.06.171.
- [72] I.A. Ibrahim, F.A. Mohamed, E.J. Lavernia, Particulate reinforced metal matrix composites - a review, *J. Mater. Sci.* 26 (1991) 1137–1156. doi:10.1007/BF00544448.
- [73] R. Ghelichi, S. Bagherifard, D. Mac Donald, M. Brochu, H. Jahed, B. Jodoin, M. Guagliano, Fatigue strength of Al alloy cold sprayed with nanocrystalline powders, *Int. J. Fatigue.* 65 (2014) 51–57. doi:10.1016/j.ijfatigue.2013.09.001.
- [74] L. Ajdelsztajn, J.M. Schoenung, B. Jodoin, G.E. Kim, Cold spray deposition of nanocrystalline aluminum alloys, *Metall. Mater. Trans. A.* 36 (2005) 657–666. doi:10.1007/s11661-005-0182-4.
- [75] Y.Y. Zhang, X.K. Wu, H. Cui, J.S. Zhang, Cold-Spray Processing of a High Density Nanocrystalline Aluminum Alloy 2009 Coating Using a Mixture of As-Atomized and As-Cryomilled Powders, *J. Therm. Spray Technol.* 20 (2011) 1125–1132. doi:10.1007/s11666-011-9652-y.
- [76] P. Richer, B. Jodoin, L. Ajdelsztajn, E.J. Lavernia, Substrate Roughness and Thickness Effects on Cold Spray Nanocrystalline Al-Mg Coatings, *J. Therm. Spray Technol.* 15 (2006) 246–254. doi:10.1361/105996306X108174.
- [77] A. Bacciochini, M.I. Radulescu, Y. Charron-Tousignant, J. Van Dyke, M. Nganbe, M. Yandouzi, J.J. Lee, B. Jodoin, Enhanced reactivity of mechanically-activated nano-scale gasless reactive materials consolidated by coldspray, *Surf. Coat. Technol.* 206 (2012) 4343–4348. doi:10.1016/j.surfcoat.2012.02.024.
- [78] J. Liu, X. Zhou, X. Zheng, H. Cui, J. Zhang, Tribological behavior of cold-sprayed nanocrystalline and conventional copper coatings, *Appl. Surf. Sci.* 258 (2012) 7490–7496. doi:10.1016/j.apsusc.2012.04.070.
- [79] L. Ajdelsztajn, B. Jodoin, J.M. Schoenung, Synthesis and mechanical properties of nanocrystalline Ni coatings produced by cold gas dynamic spraying, *Surf. Coat. Technol.* 201 (2006) 1166–1172. doi:10.1016/j.surfcoat.2006.01.037.
- [80] Q. Zhang, C.-J. Li, C.-X. Li, G.-J. Yang, S.-C. Lui, Study of oxidation behavior of nanostructured NiCrAlY bond coatings deposited by cold spraying, *Surf. Coat. Technol.* 202 (2008) 3378–3384. doi:10.1016/j.surfcoat.2007.12.028.
- [81] S.R. Bakshi, V. Singh, K. Balani, D.G. McCartney, S. Seal, A. Agarwal, Carbon nanotube reinforced aluminum composite coating via cold spraying, *Surf. Coat. Technol.* 202 (2008) 5162–5169. doi:10.1016/j.surfcoat.2008.05.042.
- [82] S. Cho, K. Takagi, H. Kwon, D. Seo, K. Ogawa, K. Kikuchi, A. Kawasaki, Multi-walled carbon nanotube-reinforced copper nanocomposite coating fabricated by low-pressure cold spray process, *Surf. Coat. Technol.* 206 (2012) 3488–3494. doi:10.1016/j.surfcoat.2012.02.021.
- [83] E.J.T. Pialago, O.K. Kwon, C.W. Park, Nucleate boiling heat transfer of R134a on cold sprayed CNT–Cu composite coatings, *Appl. Therm. Eng.* 56 (2013) 112–119. doi:10.1016/j.applthermaleng.2013.03.046.
- [84] D.J. Woo, B. Sneed, F. Peerally, F.C. Heer, L.N. Brewer, J.P. Hooper, S. Osswald, Synthesis of nanodiamond-reinforced aluminum metal composite powders and coatings using high-energy ball milling and cold spray, *Carbon.* 63 (2013) 404–415. doi:10.1016/j.carbon.2013.07.001.
- [85] D.J. Woo, F.C. Heer, L.N. Brewer, J.P. Hooper, S. Osswald, Synthesis of nanodiamond-reinforced aluminum metal matrix composites using cold-spray deposition, *Carbon.* 86 (2015) 15–25. doi:10.1016/j.carbon.2015.01.010.
- [86] S.-Q. Fan, C.-J. Li, C.-X. Li, G.-J. Liu, G.-J. Yang, L.-Z. Zhang, Preliminary Study of Performance of Dye-Sensitized Solar Cell of Nano-TiO<sub>2</sub> Coating Deposited by Vacuum Cold Spraying, *Mater. Trans.* 47 (2006) 1703–1709. doi:10.2320/matertrans.47.1703.
- [87] G.-J. Yang, K.-X. Liao, C.-J. Li, S.-Q. Fan, C.-X. Li, S. Li, Formation of Pore Structure and Its Influence on the Mass Transport Property of Vacuum Cold Sprayed TiO<sub>2</sub> Coatings Using

- Strengthened Nanostructured Powder, *J. Therm. Spray Technol.* 21 (2012) 505–513. doi:10.1007/s11666-012-9741-6.
- [88] D.-M. Chun, J.-O. Choi, C.S. Lee, I. Kanno, H. Kotera, S.-H. Ahn, Nano-particle deposition system (NPDS): Low energy solvent-free dry spray process for direct patterning of metals and ceramics at room temperature, *Int. J. Precis. Eng. Manuf.* 13 (2012) 1107–1112. doi:10.1007/s12541-012-0145-9.
- [89] T. Marrocco, D.G. McCartney, P.H. Shipway, A.J. Sturgeon, Production of Titanium Deposits by Cold-Gas Dynamic Spray: Numerical Modeling and Experimental Characterization, *J. Therm. Spray Technol.* 15 (2006) 263–272. doi:10.1361/105996306X108219.
- [90] S. Yin, Y. Xie, X. Suo, H. Liao, X. Wang, Interfacial bonding features of Ni coating on Al substrate with different surface pretreatments in cold spray, *Mater. Lett.* 138 (2015) 143–147. doi:10.1016/j.matlet.2014.10.016.
- [91] T. Hussain, D.G. McCartney, P.H. Shipway, Impact phenomena in cold-spraying of titanium onto various ferrous alloys, *Surf. Coat. Technol.* 205 (2011) 5021–5027. doi:10.1016/j.surfcoat.2011.05.003.
- [92] J. Wu, J. Yang, H. Fang, S. Yoon, C. Lee, The bond strength of Al–Si coating on mild steel by kinetic spraying deposition, *Appl. Surf. Sci.* 252 (2006) 7809–7814. doi:10.1016/j.apsusc.2005.09.015.
- [93] Steffen Marx, Alexander Paul, Cold Spray Coatings on Hard Surfaces. Other Commercial Applications, (2013). <http://www.coldsprayteam.com>.
- [94] K.-R. Ernst, J. Braeutigam, F. Gaertner, T. Klassen, Effect of Substrate Temperature on Cold-Gas-Sprayed Coatings on Ceramic Substrates, *J. Therm. Spray Technol.* 22 (2013) 422–432. doi:10.1007/s11666-012-9871-x.
- [95] J.G. Legoux, E. Irissou, C. Moreau, Effect of Substrate Temperature on the Formation Mechanism of Cold-Sprayed Aluminum, Zinc and Tin Coatings, *J. Therm. Spray Technol.* 16 (2007) 619–626. doi:10.1007/s11666-007-9091-y.
- [96] M. Fukumoto, H. Wada, K. Tanabe, M. Yamada, E. Yamaguchi, A. Niwa, M. Sugimoto, M. Izawa, Effect of Substrate Temperature on Deposition Behavior of Copper Particles on Substrate Surfaces in the Cold Spray Process, *J. Therm. Spray Technol.* 16 (2007) 643–650. doi:10.1007/s11666-007-9121-9.
- [97] M. Yu, W.-Y. Li, F.F. Wang, X.K. Suo, H.L. Liao, Effect of particle and substrate preheating on particle deformation behavior in cold spraying, *Surf. Coat. Technol.* 220 (2013) 174–178. doi:10.1016/j.surfcoat.2012.04.081.
- [98] S. Yin, X. Suo, Z. Guo, H. Liao, X. Wang, Deposition features of cold sprayed copper particles on preheated substrate, *Surf. Coat. Technol.* 268 (2015) 252–256. doi:10.1016/j.surfcoat.2014.11.009.
- [99] Y. Xie, M.-P. Planche, R. Raelison, H. Liao, X. Suo, P. Hervé, Effect of Substrate Preheating on Adhesive Strength of SS 316L Cold Spray Coatings, *J. Therm. Spray Technol.* 25 (2016) 123–130. doi:10.1007/s11666-015-0312-5.
- [100] X.K. Suo, M. Yu, W.Y. Li, M.P. Planche, H.L. Liao, Effect of Substrate Preheating on Bonding Strength of Cold-Sprayed Mg Coatings, *J. Therm. Spray Technol.* 21 (2012) 1091–1098. doi:10.1007/s11666-012-9803-9.
- [101] S. Yin, X. Suo, Y. Xie, W. Li, R. Lupoi, H. Liao, Effect of substrate temperature on interfacial bonding for cold spray of Ni onto Cu, *J. Mater. Sci.* 50 (2015) 7448–7457. doi:10.1007/s10853-015-9304-6.
- [102] Robin Kromer, Laser patterning prior-treatments in cold spraying to enhance adhesion bond strength by anchoring mechanisms, (2015).
- [103] R. Kromer, C. Verdy, S. Costil, H. Liao, Laser surface texturing to enhance adhesion bond strength of spray coatings – Cold spraying, wire-arc spraying, and atmospheric plasma spraying, *Surf. Coat. Technol.* (n.d.). doi:10.1016/j.surfcoat.2017.05.007.
- [104] T. Schmidt, F. Gärtner, H. Assadi, H. Kreye, Development of a generalized parameter window for cold spray deposition, *Acta Mater.* 54 (2006) 729–742. doi:10.1016/j.actamat.2005.10.005.

- [105] T. Schmidt, H. Assadi, F. Gärtner, H. Richter, T. Stoltenhoff, H. Kreye, T. Klassen, From Particle Acceleration to Impact and Bonding in Cold Spraying, *J. Therm. Spray Technol.* 18 (2009) 794–808. doi:10.1007/s11666-009-9357-7.
- [106] H. Assadi, T. Schmidt, H. Richter, J.-O. Kliemann, K. Binder, F. Gärtner, T. Klassen, H. Kreye, On Parameter Selection in Cold Spraying, *J. Therm. Spray Technol.* 20 (2011) 1161–1176. doi:10.1007/s11666-011-9662-9.
- [107] X.-J. Ning, J.-H. Jang, H.-J. Kim, The effects of powder properties on in-flight particle velocity and deposition process during low pressure cold spray process, *Appl. Surf. Sci.* 253 (2007) 7449–7455. doi:10.1016/j.apsusc.2007.03.031.
- [108] K.H. Ko, J.O. Choi, H. Lee, Pretreatment effect of Cu feedstock on cold-sprayed coatings, *J. Mater. Process. Technol.* 214 (2014) 1530–1535. doi:10.1016/j.jmatprotec.2014.02.020.
- [109] C.-J. Li, H.-T. Wang, Q. Zhang, G.-J. Yang, W.-Y. Li, H.L. Liao, Influence of Spray Materials and Their Surface Oxidation on the Critical Velocity in Cold Spraying, *J. Therm. Spray Technol.* 19 (2010) 95–101. doi:10.1007/s11666-009-9427-x.
- [110] T.H. Van Steenkiste, J.R. Smith, R.E. Teets, J.J. Moleski, D.W. Gorkiewicz, R.P. Tison, D.R. Marantz, K.A. Kowalsky, W.L. Riggs II, P.H. Zajchowski, B. Pilsner, R.C. McCune, K.J. Barnett, Kinetic spray coatings, *Surf. Coat. Technol.* 111 (1999) 62–71. doi:10.1016/S0257-8972(98)00709-9.
- [111] F. Gärtner, T. Stoltenhoff, T. Schmidt, H. Kreye, The Cold Spray Process and Its Potential for Industrial Applications, *J. Therm. Spray Technol.* 15 (2006) 223–232. doi:10.1361/105996306X108110.
- [112] W. Wong, P. Vo, E. Irissou, A.N. Ryabinin, J.-G. Legoux, S. Yue, Effect of Particle Morphology and Size Distribution on Cold-Sprayed Pure Titanium Coatings, *J. Therm. Spray Technol.* 22 (2013) 1140–1153. doi:10.1007/s11666-013-9951-6.
- [113] B. Jodoin, L. Ajdelsztajn, E. Sansoucy, A. Zúñiga, P. Richer, E.J. Lavernia, Effect of particle size, morphology, and hardness on cold gas dynamic sprayed aluminum alloy coatings, *Surf. Coat. Technol.* 201 (2006) 3422–3429. doi:10.1016/j.surfcoat.2006.07.232.
- [114] B. Jodoin, L. Ajdelsztajn, E. Sansoucy, A. Zúñiga, P. Richer, E.J. Lavernia, Effect of particle size, morphology, and hardness on cold gas dynamic sprayed aluminum alloy coatings, *Surf. Coat. Technol.* 201 (2006) 3422–3429. doi:10.1016/j.surfcoat.2006.07.232.
- [115] N. Cinca, J.M. Rebled, S. Estradé, F. Peiró, J. Fernández, J.M. Guilemany, Influence of the particle morphology on the Cold Gas Spray deposition behaviour of titanium on aluminum light alloys, *J. Alloys Compd.* 554 (2013) 89–96. doi:10.1016/j.jallcom.2012.11.069.
- [116] X.-T. Luo, Y.-J. Li, C.-J. Li, A comparison of cold spray deposition behavior between gas atomized and dendritic porous electrolytic Ni powders under the same spray conditions, *Mater. Lett.* 163 (2016) 58–60. doi:10.1016/j.matlet.2015.10.048.
- [117] X.-T. Luo, Y.-J. Li, C.-X. Li, G.-J. Yang, C.-J. Li, Effect of spray conditions on deposition behavior and microstructure of cold sprayed Ni coatings sprayed with a porous electrolytic Ni powder, *Surf. Coat. Technol.* 289 (2016) 85–93. doi:10.1016/j.surfcoat.2016.01.058.
- [118] M. Winnicki, A. Małachowska, A. Baszczuk, M. Rutkowska-Gorczyca, D. Kukła, M. Lachowicz, A. Ambroziak, Corrosion protection and electrical conductivity of copper coatings deposited by low-pressure cold spraying, *Surf. Coat. Technol.* (n.d.). doi:10.1016/j.surfcoat.2016.12.101.
- [119] Juha Lagerbom, Heli Koivuluoto, Jussi Larjo, Mikko Kylmälahti, Petri Vuoristo, Comparison of coatings prepared by two different cold spray processes, in: 2007.
- [120] M. Winnicki, A. Małachowska, G. Dudzik, M. Rutkowska-Gorczyca, M. Marciniak, K. Abramski, A. Ambroziak, L. Pawłowski, Numerical and experimental analysis of copper particles velocity in low-pressure cold spraying process, *Surf. Coat. Technol.* 268 (2015) 230–240. doi:10.1016/j.surfcoat.2014.11.059.
- [121] A. Małachowska, M. Winnicki, Ł. Konat, T. Piwowarczyk, L. Pawłowski, A. Ambroziak, M. Stachowicz, Possibility of spraying of copper coatings on polyamide 6 with low pressure cold spray method, *Surf. Coat. Technol.* (n.d.). doi:10.1016/j.surfcoat.2017.02.001.

- [122] J. Villafuerte, Current and future applications of cold spray technology, *Met. Finish.* 108 (2010) 37–39. doi:10.1016/S0026-0576(10)80005-4.
- [123] N.M. Chavan, M. Ramakrishna, P.S. Phani, D.S. Rao, G. Sundararajan, The influence of process parameters and heat treatment on the properties of cold sprayed silver coatings, *Surf. Coat. Technol.* 205 (2011) 4798–4807. doi:10.1016/j.surfcoat.2011.04.063.
- [124] R. Morgan, P. Fox, J. Pattison, C. Sutcliffe, W. O’Neill, Analysis of cold gas dynamically sprayed aluminium deposits, *Mater. Lett.* 58 (2004) 1317–1320. doi:10.1016/j.matlet.2003.09.048.
- [125] Q. Wang, N. Birbilis, M.-X. Zhang, Interfacial structure between particles in an aluminum deposit produced by cold spray, *Mater. Lett.* 65 (2011) 1576–1578. doi:10.1016/j.matlet.2011.03.035.
- [126] C.W. Ziemian, M.M. Sharma, B.D. Bouffard, T. Nissley, T.J. Eden, Effect of substrate surface roughening and cold spray coating on the fatigue life of AA2024 specimens, *Mater. Des.* 54 (2014) 212–221. doi:10.1016/j.matdes.2013.08.061.
- [127] K. Balani, T. Laha, A. Agarwal, J. Karthikeyan, N. Munroe, Effect of carrier gases on microstructural and electrochemical behavior of cold-sprayed 1100 aluminum coating, *Surf. Coat. Technol.* 195 (2005) 272–279. doi:10.1016/j.surfcoat.2004.06.028.
- [128] L. Ajdelsztajn, A. Zúñiga, B. Jodoin, E.J. Lavernia, Cold gas dynamic spraying of a high temperature Al alloy, *Surf. Coat. Technol.* 201 (2006) 2109–2116. doi:10.1016/j.surfcoat.2005.06.001.
- [129] K. Spencer, M.-X. Zhang, Heat treatment of cold spray coatings to form protective intermetallic layers, *Scr. Mater.* 61 (2009) 44–47. doi:10.1016/j.scriptamat.2009.03.002.
- [130] Y. Tao, T. Xiong, C. Sun, L. Kong, X. Cui, T. Li, G.-L. Song, Microstructure and corrosion performance of a cold sprayed aluminium coating on AZ91D magnesium alloy, *Corros. Sci.* 52 (2010) 3191–3197. doi:10.1016/j.corsci.2010.05.023.
- [131] H. Bu, M. Yandouzi, C. Lu, B. Jodoin, Effect of heat treatment on the intermetallic layer of cold sprayed aluminum coatings on magnesium alloy, *Surf. Coat. Technol.* 205 (2011) 4665–4671. doi:10.1016/j.surfcoat.2011.04.018.
- [132] A.P. Alkhimov, N.I. Nesterovich, A.N. Papyrin, Experimental investigation of supersonic two-phase flow over bodies, *J. Appl. Mech. Tech. Phys.* 23 (1982) 219–226. doi:10.1007/BF00911002.
- [133] H. Lee, H. Shin, S. Lee, K. Ko, Effect of gas pressure on Al coatings by cold gas dynamic spray, *Mater. Lett.* 62 (2008) 1579–1581. doi:10.1016/j.matlet.2007.09.026.
- [134] T. Hussain, D.G. McCartney, P.H. Shipway, D. Zhang, Bonding Mechanisms in Cold Spraying: The Contributions of Metallurgical and Mechanical Components, *J. Therm. Spray Technol.* 18 (2009) 364–379. doi:10.1007/s11666-009-9298-1.
- [135] S. Yin, X. Wang, X. Suo, H. Liao, Z. Guo, W. Li, C. Coddet, Deposition behavior of thermally softened copper particles in cold spraying, *Acta Mater.* 61 (2013) 5105–5118. doi:10.1016/j.actamat.2013.04.041.
- [136] P.D. Eason, J.A. Fewkes, S.C. Kennett, T.J. Eden, K. Tello, M.J. Kaufman, M. Tiryakioğlu, On the characterization of bulk copper produced by cold gas dynamic spray processing in as fabricated and annealed conditions, *Mater. Sci. Eng. A.* 528 (2011) 8174–8178. doi:10.1016/j.msea.2011.07.012.
- [137] H.-J. Choi, M. Lee, J.Y. Lee, Application of a cold spray technique to the fabrication of a copper canister for the geological disposal of CANDU spent fuels, *Nucl. Eng. Des.* 240 (2010) 2714–2720. doi:10.1016/j.nucengdes.2010.06.038.
- [138] P. Poza, C.J. Múnez, M.A. Garrido-Maneiro, S. Vezzù, S. Rech, A. Trentin, Mechanical properties of Inconel 625 cold-sprayed coatings after laser remelting. Depth sensing indentation analysis, *Surf. Coat. Technol.* 243 (2014) 51–57. doi:10.1016/j.surfcoat.2012.03.018.
- [139] D. Levasseur, S. Yue, M. Brochu, Pressureless sintering of cold sprayed Inconel 718 deposit, *Mater. Sci. Eng. A.* 556 (2012) 343–350. doi:10.1016/j.msea.2012.06.097.

- [140] Y. Zou, W. Qin, E. Irissou, J.-G. Legoux, S. Yue, J.A. Szipunar, Dynamic recrystallization in the particle/particle interfacial region of cold-sprayed nickel coating: Electron backscatter diffraction characterization, *Scr. Mater.* 61 (2009) 899–902. doi:10.1016/j.scriptamat.2009.07.020.
- [141] X. Meng, J. Zhang, J. Zhao, Y. Liang, Y. Zhang, Influence of Gas Temperature on Microstructure and Properties of Cold Spray 304SS Coating, *J. Mater. Sci. Technol.* 27 (2011) 809–815. doi:10.1016/S1005-0302(11)60147-3.
- [142] A. Sova, S. Grigoriev, A. Okunkova, I. Smurov, Cold spray deposition of 316L stainless steel coatings on aluminium surface with following laser post-treatment, *Surf. Coat. Technol.* 235 (2013) 283–289. doi:10.1016/j.surfcoat.2013.07.052.
- [143] M. Villa, S. Dosta, J.M. Guilemany, Optimization of 316L stainless steel coatings on light alloys using Cold Gas Spray, *Surf. Coat. Technol.* 235 (2013) 220–225. doi:10.1016/j.surfcoat.2013.07.036.
- [144] G. Bolelli, B. Bonferroni, H. Koivuluoto, L. Lusvarghi, P. Vuoristo, Depth-sensing indentation for assessing the mechanical properties of cold-sprayed Ta, *Surf. Coat. Technol.* 205 (2010) 2209–2217. doi:10.1016/j.surfcoat.2010.08.146.
- [145] R.S. Lima, A. Kucuk, C.C. Berndt, J. Karthikeyan, C.M. Kay, J. Lindemann, Deposition efficiency, mechanical properties and coating roughness in cold-sprayed titanium, *J. Mater. Sci. Lett.* 21 (2002) 1687–1689. doi:10.1023/A:1020833011448.
- [146] C.K.S. Moy, J. Cairney, G. Ranzi, M. Jahedi, S.P. Ringer, Investigating the microstructure and composition of cold gas-dynamic spray (CGDS) Ti powder deposited on Al 6063 substrate, *Surf. Coat. Technol.* 204 (2010) 3739–3749. doi:10.1016/j.surfcoat.2010.04.016.
- [147] C.-J. Li, W.-Y. Li, Deposition characteristics of titanium coating in cold spraying, *Surf. Coat. Technol.* 167 (2003) 278–283. doi:10.1016/S0257-8972(02)00919-2.
- [148] H.-R. Wang, W.-Y. Li, L. Ma, J. Wang, Q. Wang, Corrosion behavior of cold sprayed titanium protective coating on 1Cr13 substrate in seawater, *Surf. Coat. Technol.* 201 (2007) 5203–5206. doi:10.1016/j.surfcoat.2006.07.104.
- [149] J. Ajaja, D. Goldbaum, R.R. Chromik, Characterization of Ti cold spray coatings by indentation methods, *Acta Astronaut.* 69 (2011) 923–928. doi:10.1016/j.actaastro.2011.06.012.
- [150] S.H. Zahiri, C.I. Antonio, M. Jahedi, Elimination of porosity in directly fabricated titanium via cold gas dynamic spraying, *J. Mater. Process. Technol.* 209 (2009) 922–929. doi:10.1016/j.jmatprotec.2008.03.005.
- [151] J. Cizek, O. Kovarik, J. Siegl, K.A. Khor, I. Dlouhy, Influence of plasma and cold spray deposited Ti Layers on high-cycle fatigue properties of Ti6Al4V substrates, *Surf. Coat. Technol.* 217 (2013) 23–33. doi:10.1016/j.surfcoat.2012.11.067.
- [152] W.-Y. Li, C.-J. Li, G.-J. Yang, Effect of impact-induced melting on interface microstructure and bonding of cold-sprayed zinc coating, *Appl. Surf. Sci.* 257 (2010) 1516–1523. doi:10.1016/j.apsusc.2010.08.089.
- [153] W.-Y. Li, C. Zhang, X.P. Guo, G. Zhang, H.L. Liao, C.-J. Li, C. Coddet, Effect of standoff distance on coating deposition characteristics in cold spraying, *Mater. Des.* 29 (2008) 297–304. doi:10.1016/j.matdes.2007.02.005.
- [154] Z.B. Zhao, B.A. Gillispie, J.R. Smith, Coating deposition by the kinetic spray process, *Surf. Coat. Technol.* 200 (2006) 4746–4754. doi:10.1016/j.surfcoat.2005.04.033.
- [155] J. Pattison, S. Celotto, A. Khan, W. O’Neill, Standoff distance and bow shock phenomena in the Cold Spray process, *Surf. Coat. Technol.* 202 (2008) 1443–1454. doi:10.1016/j.surfcoat.2007.06.065.
- [156] F. Raletz, M. Vardelle, G. Ezo’o, Critical particle velocity under cold spray conditions, *Surf. Coat. Technol.* 201 (2006) 1942–1947. doi:10.1016/j.surfcoat.2006.04.061.
- [157] C.-J. Li, W.-Y. Li, Y.-Y. Wang, Effect of Spray Angle on Deposition Characteristics in Cold Spraying, in: *Proc. Int. Therm. Spray Conf.*, C. Moreau and B. Marple, Orlando, Florida, 2003: pp. 91–96.

- [158] H. Fukanuma, N. Ohno, B. Sun, R. Huang, In-flight particle velocity measurements with DPV-2000 in cold spray, *Surf. Coat. Technol.* 201 (2006) 1935–1941. doi:10.1016/j.surfcoat.2006.04.035.
- [159] H. Fukanuma, R. Huang, Development of High Temperature Gas Heater in the Cold Spray Coating System, in: *Proc. Int. Therm. Spray Conf.*, B.R. Marple, M.M. Hyland, Y.-C. Lau, C.-J. Li, R.S. Lima, G. Montavon, editors, 2009: pp. 267–272. doi:10.1361/cp2009itsc0267.
- [160] W.-Y. Li, C. Zhang, H.-T. Wang, X.P. Guo, H.L. Liao, C.-J. Li, C. Coddet, Significant influences of metal reactivity and oxide films at particle surfaces on coating microstructure in cold spraying, *Appl. Surf. Sci.* 253 (2007) 3557–3562. doi:10.1016/j.apsusc.2006.07.063.
- [161] M. Yandouzi, P. Richer, B. Jodoin, SiC particulate reinforced Al–12Si alloy composite coatings produced by the pulsed gas dynamic spray process: Microstructure and properties, *Surf. Coat. Technol.* 203 (2009) 3260–3270. doi:10.1016/j.surfcoat.2009.04.001.
- [162] X.-J. Ning, J.-H. Kim, H.-J. Kim, C. Lee, Characteristics and heat treatment of cold-sprayed Al–Sn binary alloy coatings, *Appl. Surf. Sci.* 255 (2009) 3933–3939. doi:10.1016/j.apsusc.2008.10.074.
- [163] X.-J. Ning, J.-H. Jang, H.-J. Kim, C.-J. Li, C. Lee, Cold spraying of Al–Sn binary alloy: Coating characteristics and particle bonding features, *Surf. Coat. Technol.* 202 (2008) 1681–1687. doi:10.1016/j.surfcoat.2007.07.026.
- [164] E. Sansoucy, G.E. Kim, A.L. Moran, B. Jodoin, Mechanical Characteristics of Al–Co–Ce Coatings Produced by the Cold Spray Process, *J. Therm. Spray Technol.* 16 (2007) 651–660. doi:10.1007/s11666-007-9099-3.
- [165] P. Coddet, C. Verdy, C. Coddet, F. Lecouturier, F. Debray, Mechanical properties of Cold Spray deposited NARloy-Z copper alloy, *Surf. Coat. Technol.* 232 (2013) 652–657. doi:10.1016/j.surfcoat.2013.06.062.
- [166] S.V. Raj, C. Barrett, J. Karthikeyan, R. Garlick, Comparison of the cyclic oxidation behavior of cold sprayed CuCrAl-coated and uncoated GRCop-84 substrates for space launch vehicles, *Surf. Coat. Technol.* 201 (2007) 7222–7234. doi:10.1016/j.surfcoat.2007.01.034.
- [167] W.-Y. Li, C.-J. Li, H. Liao, C. Coddet, Effect of heat treatment on the microstructure and microhardness of cold-sprayed tin bronze coating, *Appl. Surf. Sci.* 253 (2007) 5967–5971. doi:10.1016/j.apsusc.2006.12.108.
- [168] X. Guo, G. Zhang, W.-Y. Li, L. Dembinski, Y. Gao, H. Liao, C. Coddet, Microstructure, microhardness and dry friction behavior of cold-sprayed tin bronze coatings, *Appl. Surf. Sci.* 254 (2007) 1482–1488. doi:10.1016/j.apsusc.2007.07.026.
- [169] N. Cinca, E. López, S. Dosta, J.M. Guilemany, Study of stellite-6 deposition by cold gas spraying, *Surf. Coat. Technol.* 232 (2013) 891–898. doi:10.1016/j.surfcoat.2013.06.120.
- [170] N. Cinca, J.M. Guilemany, Structural and properties characterization of stellite coatings obtained by cold gas spraying, *Surf. Coat. Technol.* 220 (2013) 90–97. doi:10.1016/j.surfcoat.2012.11.026.
- [171] S. Rech, A. Surpi, S. Vezzù, A. Patelli, A. Trentin, J. Glor, J. Frodelius, L. Hultman, P. Eklund, Cold-spray deposition of Ti2AlC coatings, *Vacuum.* 94 (2013) 69–73. doi:10.1016/j.vacuum.2013.01.023.
- [172] D.-M. Chun, J.-O. Choi, C.S. Lee, S.-H. Ahn, Effect of stand-off distance for cold gas spraying of fine ceramic particles (< 5  $\mu\text{m}$ ) under low vacuum and room temperature using nano-particle deposition system (NPDS), *Surf. Coat. Technol.* 206 (2012) 2125–2132. doi:10.1016/j.surfcoat.2011.09.043.
- [173] P. Richer, M. Yandouzi, L. Beauvais, B. Jodoin, Oxidation behaviour of CoNiCrAlY bond coats produced by plasma, HVOF and cold gas dynamic spraying, *Surf. Coat. Technol.* 204 (2010) 3962–3974. doi:10.1016/j.surfcoat.2010.03.043.
- [174] A. Bonadei, T. Marrocco, Cold sprayed MCrAlY + X coating for gas turbine blades and vanes, *Surf. Coat. Technol.* 242 (2014) 200–206. doi:10.1016/j.surfcoat.2013.08.019.
- [175] H.-J. Kim, C.-H. Lee, S.-Y. Hwang, Fabrication of WC–Co coatings by cold spray deposition, *Surf. Coat. Technol.* 191 (2005) 335–340. doi:10.1016/j.surfcoat.2004.04.058.

- [176] T.S. Price, P.H. Shipway, D.G. McCartney, E. Calla, D. Zhang, A Method for Characterizing the Degree of Inter-particle Bond Formation in Cold Sprayed Coatings, *J. Therm. Spray Technol.* 16 (2007) 566–570. doi:10.1007/s11666-007-9070-3.
- [177] M. Bashirzadeh, F. Azarmi, C.P. Leither, G. Karami, Investigation on relationship between mechanical properties and microstructural characteristics of metal matrix composites fabricated by cold spraying technique, *Appl. Surf. Sci.* 275 (2013) 208–216. doi:10.1016/j.apsusc.2012.12.166.
- [178] H.-T. Wang, C.-J. Li, G.-J. Yang, C.-X. Li, Cold spraying of Fe/Al powder mixture: Coating characteristics and influence of heat treatment on the phase structure, *Appl. Surf. Sci.* 255 (2008) 2538–2544. doi:10.1016/j.apsusc.2008.07.127.
- [179] H.Y. Lee, S.H. Jung, S.Y. Lee, K.H. Ko, Fabrication of cold sprayed Al-intermetallic compounds coatings by post annealing, *Mater. Sci. Eng. A.* 433 (2006) 139–143. doi:10.1016/j.msea.2006.06.044.
- [180] T. Novoselova, P. Fox, R. Morgan, W. O’Neill, Experimental study of titanium/aluminium deposits produced by cold gas dynamic spray, *Surf. Coat. Technol.* 200 (2006) 2775–2783. doi:10.1016/j.surfcoat.2004.10.133.
- [181] H.Y. Lee, S.H. Jung, S.Y. Lee, K.H. Ko, Alloying of cold-sprayed Al–Ni composite coatings by post-annealing, *Appl. Surf. Sci.* 253 (2007) 3496–3502. doi:10.1016/j.apsusc.2006.07.053.
- [182] H. Lee, S. Lee, K. Ko, Annealing effects on the intermetallic compound formation of cold sprayed Ni, Al coatings, *J. Mater. Process. Technol.* 209 (2009) 937–943. doi:10.1016/j.jmatprotec.2008.03.001.
- [183] H. Bu, M. Yandouzi, C. Lu, D. MacDonald, B. Jodoin, Cold spray blended Al + Mg<sub>17</sub>Al<sub>12</sub> coating for corrosion protection of AZ91D magnesium alloy, *Surf. Coat. Technol.* 207 (2012) 155–162. doi:10.1016/j.surfcoat.2012.06.050.
- [184] H.Y. Lee, S.H. Jung, S.Y. Lee, Y.H. You, K.H. Ko, Correlation between Al<sub>2</sub>O<sub>3</sub> particles and interface of Al–Al<sub>2</sub>O<sub>3</sub> coatings by cold spray, *Appl. Surf. Sci.* 252 (2005) 1891–1898. doi:10.1016/j.apsusc.2005.03.148.
- [185] E. Irissou, J.-G. Legoux, B. Arsenault, C. Moreau, Investigation of Al–Al<sub>2</sub>O<sub>3</sub> Cold Spray Coating Formation and Properties, *J. Therm. Spray Technol.* 16 (2007) 661–668. doi:10.1007/s11666-007-9086-8.
- [186] Q. Wang, K. Spencer, N. Birbilis, M.-X. Zhang, The influence of ceramic particles on bond strength of cold spray composite coatings on AZ91 alloy substrate, *Surf. Coat. Technol.* 205 (2010) 50–56. doi:10.1016/j.surfcoat.2010.06.008.
- [187] K. Spencer, D.M. Fabijanic, M.-X. Zhang, The use of Al–Al<sub>2</sub>O<sub>3</sub> cold spray coatings to improve the surface properties of magnesium alloys, *Surf. Coat. Technol.* 204 (2009) 336–344. doi:10.1016/j.surfcoat.2009.07.032.
- [188] Y. Tao, T. Xiong, C. Sun, H. Jin, H. Du, T. Li, Effect of  $\alpha$ -Al<sub>2</sub>O<sub>3</sub> on the properties of cold sprayed Al/ $\alpha$ -Al<sub>2</sub>O<sub>3</sub> composite coatings on AZ91D magnesium alloy, *Appl. Surf. Sci.* 256 (2009) 261–266. doi:10.1016/j.apsusc.2009.08.012.
- [189] H.Y. Lee, Y.H. Yu, Y.C. Lee, Y.P. Hong, K.H. Ko, Cold Spray of SiC and Al<sub>2</sub>O<sub>3</sub> With Soft Metal Incorporation: A Technical Contribution, *J. Therm. Spray Technol.* 13 (2004) 184–189. doi:10.1361/10599630419355.
- [190] A. Bacciochini, M.I. Radulescu, M. Yandouzi, G. Maines, J.J. Lee, B. Jodoin, Reactive structural materials consolidated by cold spray: Al–CuO thermite, *Surf. Coat. Technol.* 226 (2013) 60–67. doi:10.1016/j.surfcoat.2013.03.036.
- [191] E. Sansoucy, P. Marcoux, L. Ajdelsztajn, B. Jodoin, Properties of SiC-reinforced aluminum alloy coatings produced by the cold gas dynamic spraying process, *Surf. Coat. Technol.* 202 (2008) 3988–3996. doi:10.1016/j.surfcoat.2008.02.017.
- [192] E. Sansoucy, L. Ajdelsztajn, B. Jodoin, P. Marcoux, Properties of SiC-Reinforced Aluminum Alloy Coatings Produced by the Cold Spray Deposition Process, in: *Therm. Spray 2007 Glob. Coat. Solut.*, ASM International, 2007: pp. 37–42. <http://www.asminternational.org/web/detroit-chapter/search/>

- /journal\_content/56/10192/CP2007ITSC0037/PUBLICATION;jsessionid=72C1438B99C672EF5627613BAB27E19B?p\_p\_id=56\_INSTANCE\_0000&p\_p\_lifecycle=0&p\_p\_state=maximized&p\_p\_mode=view (accessed April 30, 2016).
- [193] W.-Y. Li, G. Zhang, H.L. Liao, C. Coddet, Characterizations of cold sprayed TiN particle reinforced Al2319 composite coating, *J. Mater. Process. Technol.* 202 (2008) 508–513. doi:10.1016/j.jmatprotec.2007.09.045.
- [194] O. Meydanoglu, B. Jodoin, E.S. Kayali, Microstructure, mechanical properties and corrosion performance of 7075 Al matrix ceramic particle reinforced composite coatings produced by the cold gas dynamic spraying process, *Surf. Coat. Technol.* 235 (2013) 108–116. doi:10.1016/j.surfcoat.2013.07.020.
- [195] X. Guo, G. Zhang, W. Li, Y. Gao, H. Liao, C. Coddet, Investigation of the microstructure and tribological behavior of cold-sprayed tin-bronze-based composite coatings, *Appl. Surf. Sci.* 255 (2009) 3822–3828. doi:10.1016/j.apsusc.2008.10.041.
- [196] G.-J. Yang, H.-T. Wang, C.-J. Li, C.-X. Li, Effect of annealing on the microstructure and erosion performance of cold-sprayed FeAl intermetallic coatings, *Surf. Coat. Technol.* 205 (2011) 5502–5509. doi:10.1016/j.surfcoat.2011.06.033.
- [197] N. Sanpo, M.L. Tan, P. Cheang, K.A. Khor, Antibacterial Property of Cold-Sprayed HA-Ag/PEEK Coating, *J. Therm. Spray Technol.* 18 (2008) 10–15. doi:10.1007/s11666-008-9283-0.
- [198] X. Zhou, P. Mohanty, Electrochemical behavior of cold sprayed hydroxyapatite/titanium composite in Hanks' solution, *Electrochimica Acta.* 65 (2012) 134–140. doi:10.1016/j.electacta.2012.01.018.
- [199] J. Sun, Y. Han, K. Cui, Innovative fabrication of porous titanium coating on titanium by cold spraying and vacuum sintering, *Mater. Lett.* 62 (2008) 3623–3625. doi:10.1016/j.matlet.2008.04.011.
- [200] S.W. Dean, J.K. Potter, R.A. Yetter, T.J. Eden, V. Champagne, M. Trexler, Energetic intermetallic materials formed by cold spray, *Intermetallics.* 43 (2013) 121–130. doi:10.1016/j.intermet.2013.07.019.
- [201] W.-Y. Li, C. Zhang, H. Liao, J. Li, C. Coddet, Characterizations of cold-sprayed Nickel–Alumina composite coating with relatively large Nickel-coated Alumina powder, *Surf. Coat. Technol.* 202 (2008) 4855–4860. doi:10.1016/j.surfcoat.2008.04.076.
- [202] H.X. Hu, S.L. Jiang, Y.S. Tao, T.Y. Xiong, Y.G. Zheng, Cavitation erosion and jet impingement erosion mechanism of cold sprayed Ni–Al<sub>2</sub>O<sub>3</sub> coating, *Nucl. Eng. Des.* 241 (2011) 4929–4937. doi:10.1016/j.nucengdes.2011.09.038.
- [203] C. Feng, V. Guipont, M. Jeandin, O. Amsellem, F. Pauchet, R. Saenger, S. Bucher, C. Iacob, B4C/Ni Composite Coatings Prepared by Cold Spray of Blended or CVD-Coated Powders, *J. Therm. Spray Technol.* 21 (2012) 561–570. doi:10.1007/s11666-012-9774-x.
- [204] X.-T. Luo, G.-J. Yang, C.-J. Li, Multiple strengthening mechanisms of cold-sprayed cBNp/NiCrAl composite coating, *Surf. Coat. Technol.* 205 (2011) 4808–4813. doi:10.1016/j.surfcoat.2011.04.065.
- [205] K.H. Ko, H. Lee, J.O. Choi, Effect of Sn particle size on the intermetallic compound formations of cold sprayed Sn–Ni coatings, *Appl. Surf. Sci.* 257 (2011) 2970–2977. doi:10.1016/j.apsusc.2010.10.102.
- [206] K. Spencer, D.M. Fabijanac, M.-X. Zhang, The influence of Al<sub>2</sub>O<sub>3</sub> reinforcement on the properties of stainless steel cold spray coatings, *Surf. Coat. Technol.* 206 (2012) 3275–3282. doi:10.1016/j.surfcoat.2012.01.031.
- [207] B. AL-Mangour, R. Mongrain, E. Irissou, S. Yue, Improving the strength and corrosion resistance of 316L stainless steel for biomedical applications using cold spray, *Surf. Coat. Technol.* 216 (2013) 297–307. doi:10.1016/j.surfcoat.2012.11.061.
- [208] T. Novoselova, S. Celotto, R. Morgan, P. Fox, W. O'Neill, Formation of TiAl intermetallics by heat treatment of cold-sprayed precursor deposits, *J. Alloys Compd.* 436 (2007) 69–77. doi:10.1016/j.jallcom.2006.06.101.

- [209] L. SHEN, L. KONG, T. XIONG, H. DU, T. LI, Preparation of TiAl<sub>3</sub>-Al composite coating by cold spraying, *Trans. Nonferrous Met. Soc. China*. 19 (2009) 879–882. doi:10.1016/S1003-6326(08)60369-6.
- [210] H.-K. Kang, S.B. Kang, Tungsten/copper composite deposits produced by a cold spray, *Scr. Mater.* 49 (2003) 1169–1174. doi:10.1016/j.scriptamat.2003.08.023.
- [211] N.M. Melendez, V.V. Narulkar, G.A. Fisher, A.G. McDonald, Effect of reinforcing particles on the wear rate of low-pressure cold-sprayed WC-based MMC coatings, *Wear*. 306 (2013) 185–195. doi:10.1016/j.wear.2013.08.006.
- [212] N.M. Melendez, A.G. McDonald, Development of WC-based metal matrix composite coatings using low-pressure cold gas dynamic spraying, *Surf. Coat. Technol.* 214 (2013) 101–109. doi:10.1016/j.surfcoat.2012.11.010.
- [213] X.L. Zhou, S.J. Mou, X.K. Wu, J.S. Zhang, Deposition behavior of mixed binary metallic powders in cold spraying process, *Appl. Surf. Sci.* 257 (2011) 10628–10633. doi:10.1016/j.apsusc.2011.07.061.
- [214] J. Morimoto, T. Onoda, Y. Sasaki, N. Abe, Improvement of solid cold sprayed TiO<sub>2</sub>-Zn coating with direct diode laser, *Vacuum*. 73 (2004) 527–532. doi:10.1016/j.vacuum.2003.12.157.
- [215] H.-J. Kim, C.-H. Lee, S.-Y. Hwang, Superhard nano WC-12%Co coating by cold spray deposition, *Mater. Sci. Eng. A*. 391 (2005) 243–248. doi:10.1016/j.msea.2004.08.082.
- [216] C.-J. Li, G.-J. Yang, P.-H. Gao, J. Ma, Y.-Y. Wang, C.-X. Li, Characterization of Nanostructured WC-Co Deposited by Cold Spraying, *J. Therm. Spray Technol.* 16 (2007) 1011–1020. doi:10.1007/s11666-007-9096-6.
- [217] G.-J. Yang, C.-J. Li, F. Han, W.-Y. Li, A. Ohmori, Low temperature deposition and characterization of TiO<sub>2</sub> photocatalytic film through cold spray, *Appl. Surf. Sci.* 254 (2008) 3979–3982. doi:10.1016/j.apsusc.2007.12.016.
- [218] Y. Liu, Y.-Y. Wang, G.-J. Yang, J.-J. Feng, K. Kusumoto, Effect of Nano-Sized TiN Additions on the Electrical Properties of Vacuum Cold Sprayed SiC Coatings, *J. Therm. Spray Technol.* 19 (2010) 1238–1243. doi:10.1007/s11666-010-9544-6.
- [219] J.H. Lee, H.L. Jang, K.M. Lee, H.-R. Baek, K. Jin, K.S. Hong, J.H. Noh, H.-K. Lee, In vitro and in vivo evaluation of the bioactivity of hydroxyapatite-coated polyetheretherketone biocomposites created by cold spray technology, *Acta Biomater.* 9 (2013) 6177–6187. doi:10.1016/j.actbio.2012.11.030.

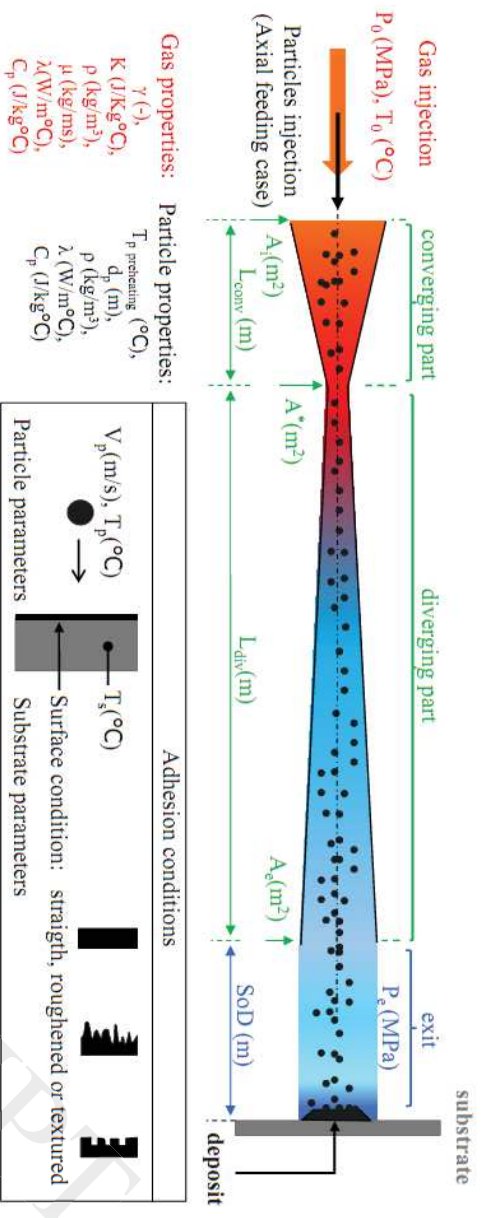


Fig. 1. Generic behaviour of the cold spray method and its main process parameters.

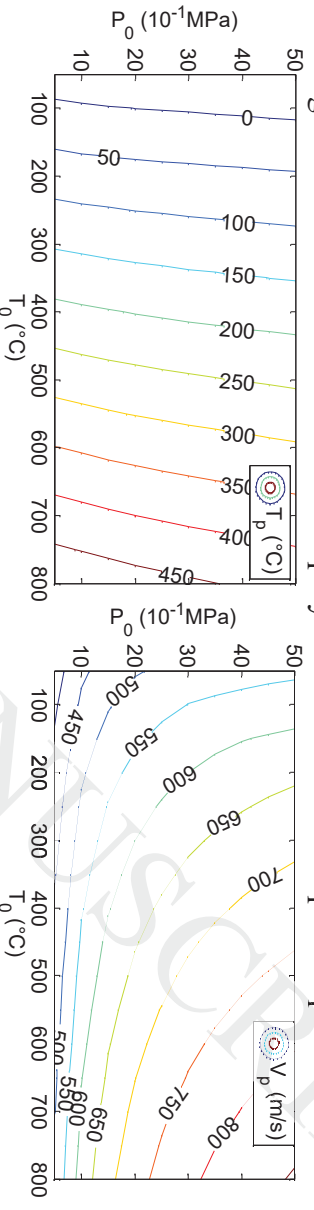


Fig. 2. Typical useful depiction of  $T_p$  and  $V_p$  depending on the variations of gas input parameters (case of air, throat = 1.6 mm,  $L_{\text{div}} = 172$  mm, Al particle with  $d_p = 40$   $\mu\text{m}$ ).



Fig. 3. Schematic procedure used to predict and/or to optimise the deposition efficiency depending on the main CGDS process parameters, as reported in the literature.

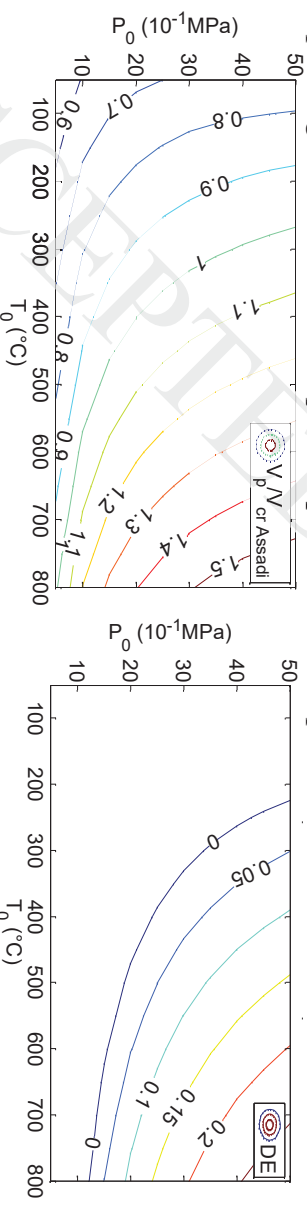


Fig. 4. Deposition range the  $V_p/V_{\text{cr}}$  ratio computed using  $V_{\text{cr}}$  model of Assadi *et al.* [4] and using a DE model from [53] (case of air, throat = 1.6 mm,  $L_{\text{div}} = 172$  mm, Al particle with  $d_p = 40$   $\mu\text{m}$ ).

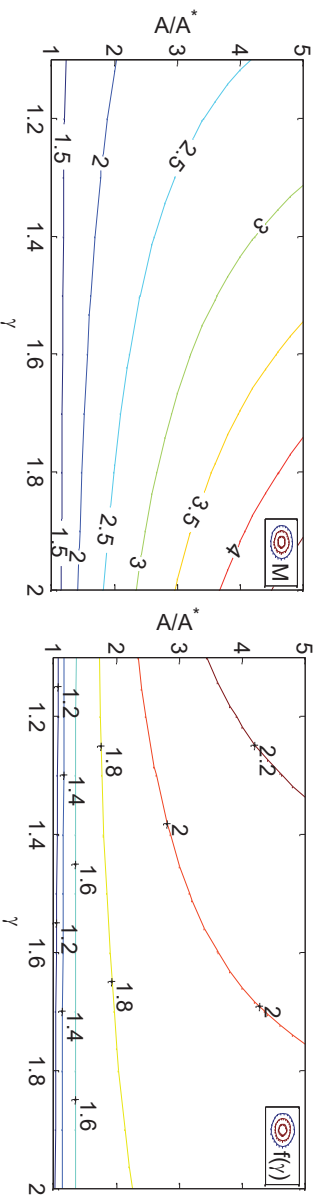


Fig. 5. Influence of  $\gamma$  on the Mach number and on the term  $f(\gamma)$ .

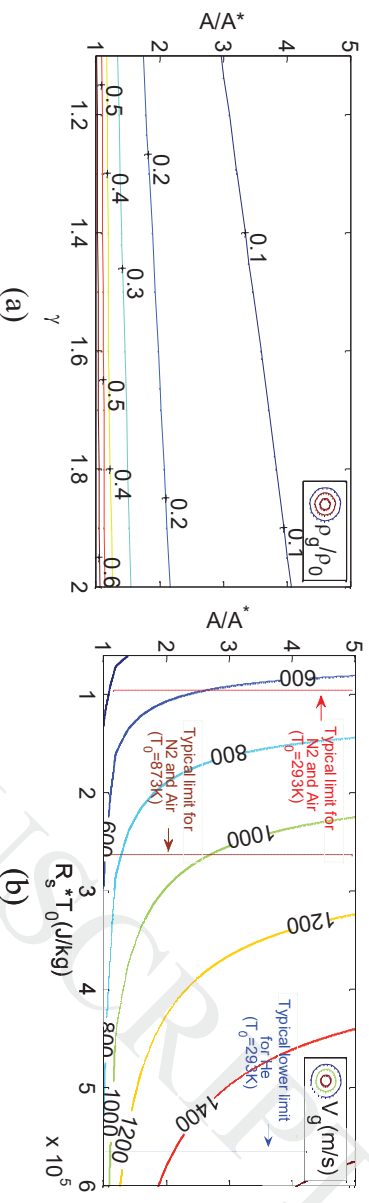


Fig. 6. (a) Influence of  $\gamma$  on the gas density ratio and (b) influence of  $R_s T_0$  revealing the typical limitations of gas velocity due to the value of  $R_s$ .

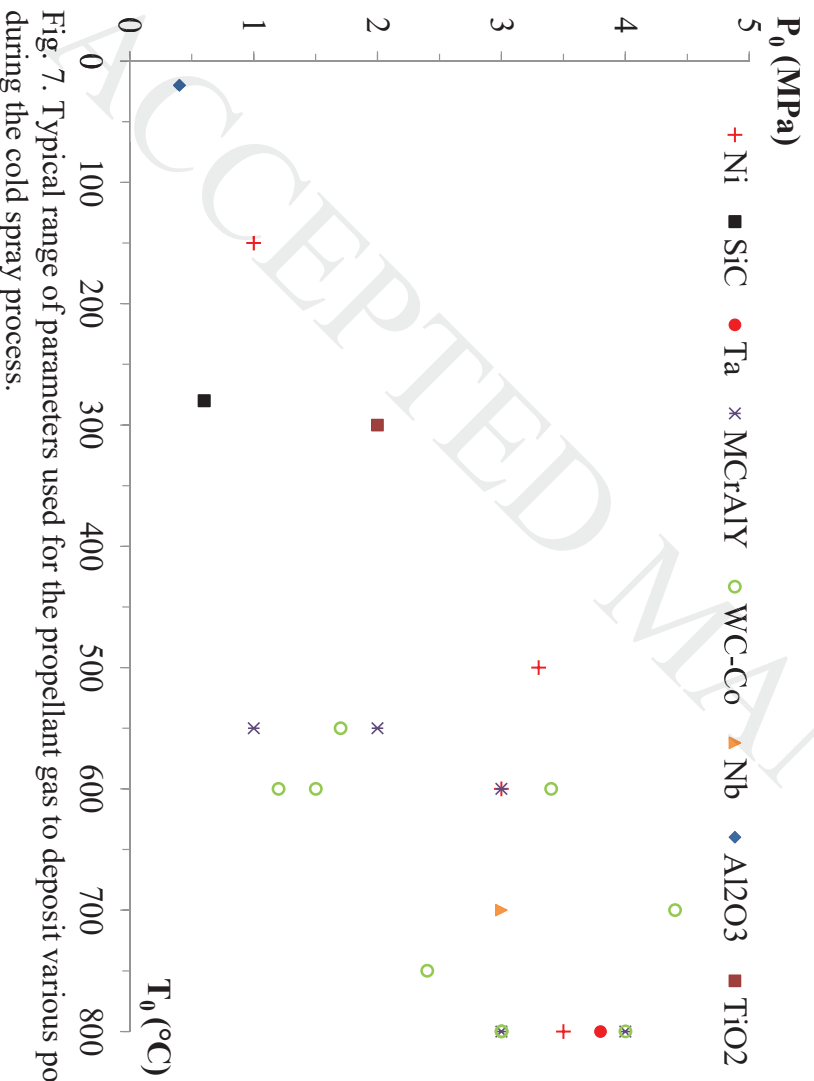
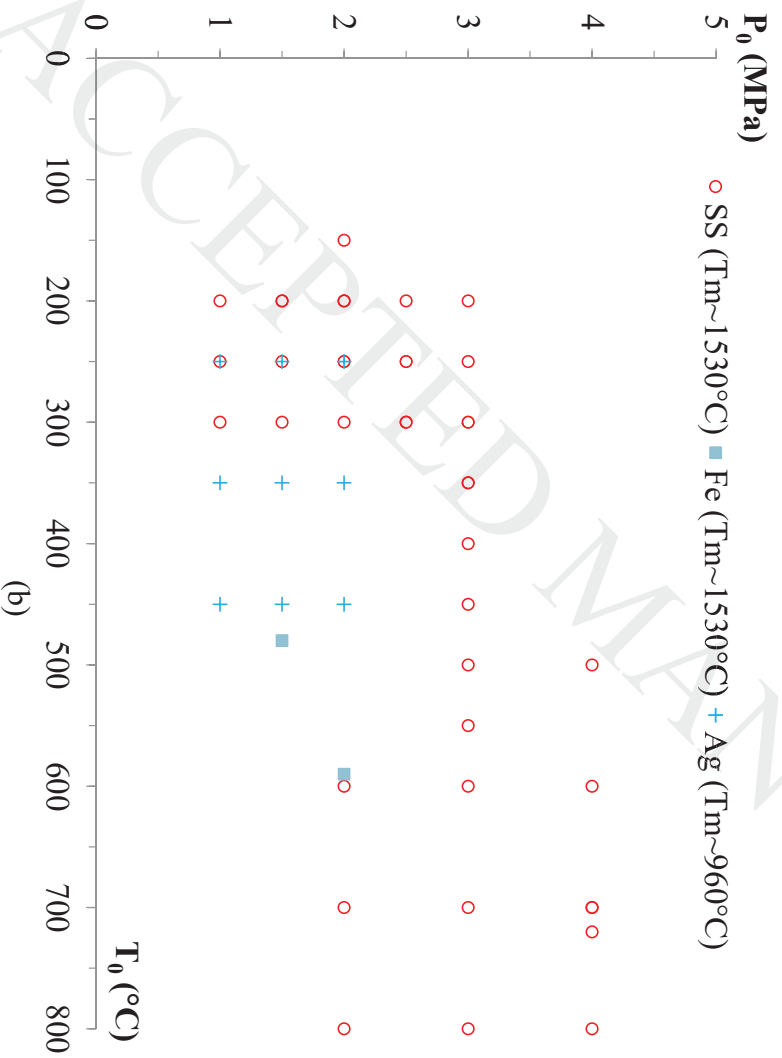
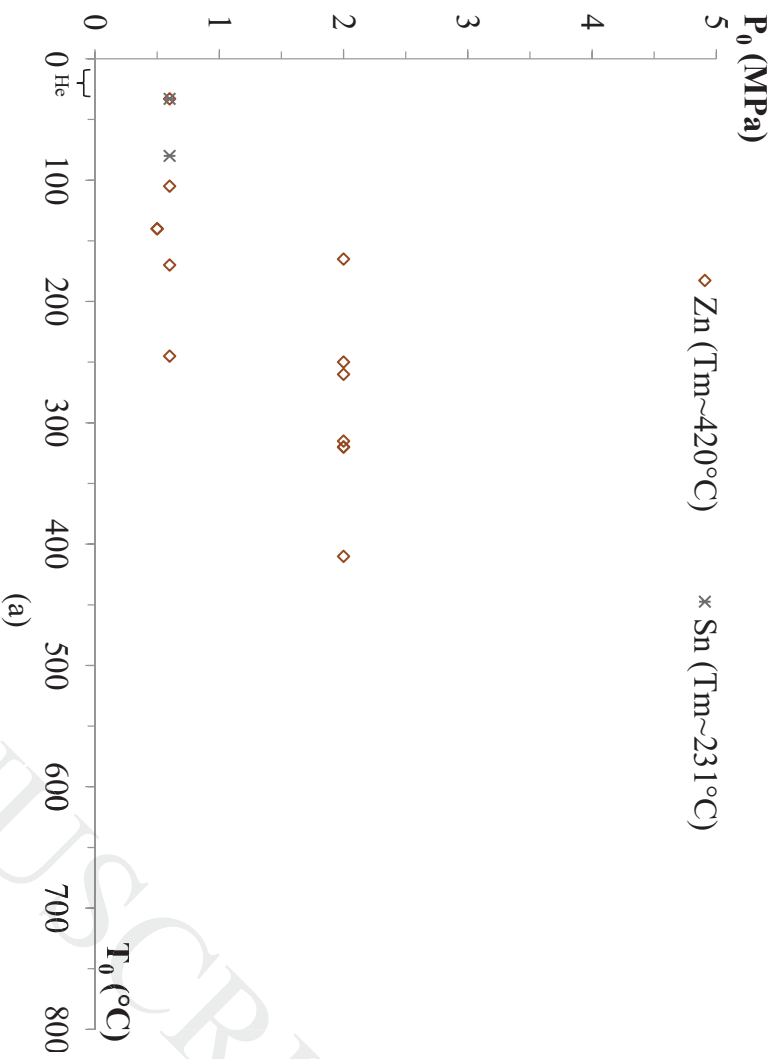


Fig. 7. Typical range of parameters used for the propellant gas to deposit various powders during the cold spray process.



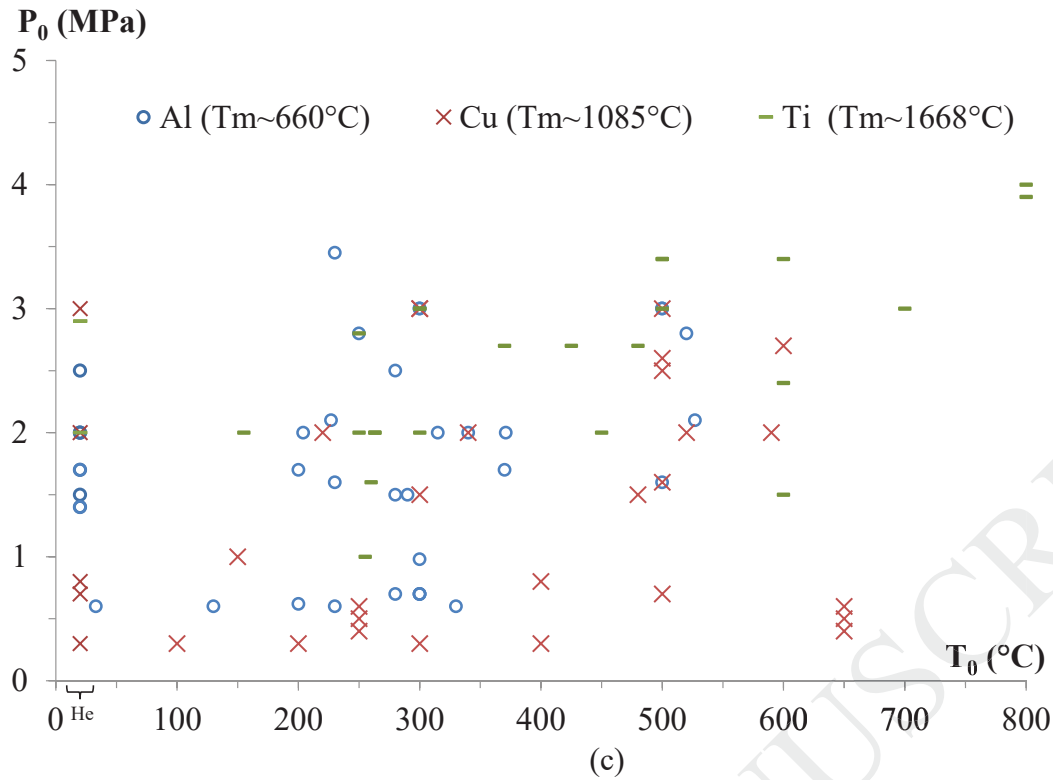


Fig. 8. Typical  $(P_0, T_0)$  parameter sets for the powders of (a) Zn and Sn; (b) Stainless steel (SS), Fe and Ag and (c) Al, Cu and Ti.

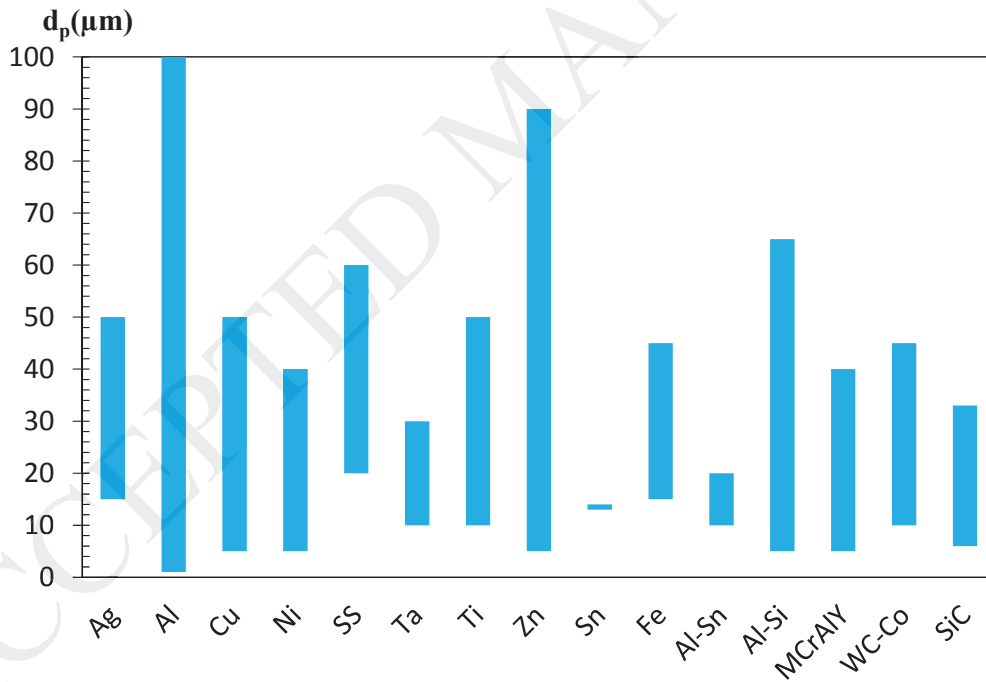


Fig. 9. Typical range of powder diameters used for various materials in CGDS experiments.

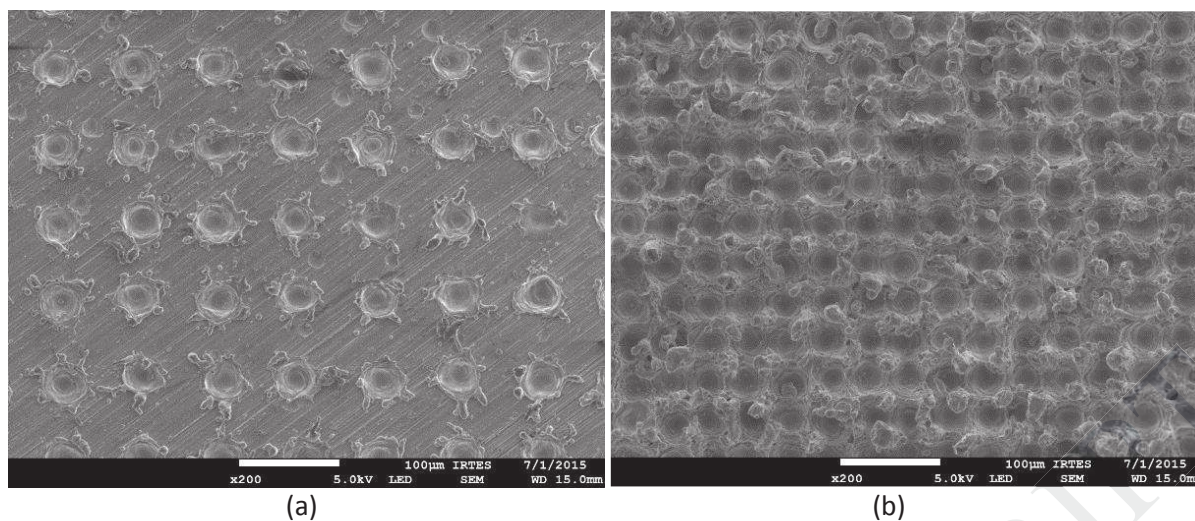


Fig. 10. Typical pattern on the Al surfaces produced using the laser texturing method: (a) a weakly textured surface (Texture 1) and (b) a highly textured surface (Texture 2) [102,103].

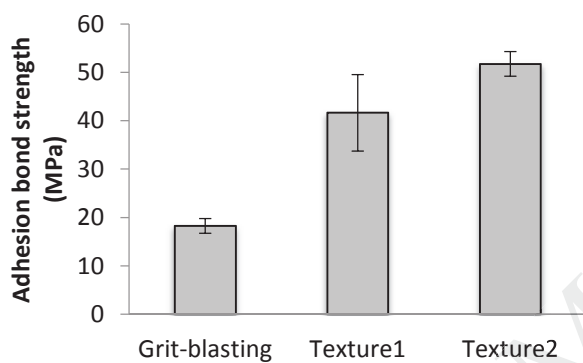


Fig. 11. Laser texturing effect on bonding strength for the cold sprayed Al powder onto an Al substrate [102,103].

Table 1. Specific heat ratio ( $\gamma$ ) and specific gas constant ( $R_s$ ) of the air,  $N_2$  and He gases.

	Air	Nitrogen	Helium
$\gamma$ (-)	1.4	1.4	1.66
$R_s$ ( $J.kg^{-1}.K^{-1}$ )	287	297	2077

Table 2. Effect of surface roughening on the bonding strength ( $\sigma_{BS}$ ) in cold spraying.

Combination	Cu/Al [91]			Ni/Al [90]			Ti/Ti6Al4V [89]		
	Ra ( $\mu m$ )	$\sigma_{BS}$ (MPa)	$d_p$ ( $\mu m$ )	Ra ( $\mu m$ )	$\sigma_{BS}$ (MPa)	$d_p$ ( $\mu m$ )	Ra ( $\mu m$ )	$\sigma_{BS}$ (MPa)	$d_p$ ( $\mu m$ )
Polished	0.05	57		0.36	~25		0.04	~22.5	
Grounded	0.4	56	5-25	2.12	~25	10-45	0.21	~22	5-45
Grit-blasted	3.9	35		6.35	~19		2.66	~8	

## Appendices: comprehensive review of CGDS processing data

### A1. Deposit with a single powder

Powder	$d_p$ ( $\mu\text{m}$ )	gas	$P_0$ (MPa)	$T_0$ ( $^{\circ}\text{C}$ )	Q (g/mn)	SoD (mm)	Nozzle parameters			$V_{\text{nozzle}}^2$ (mm/s)	Substrate	Ref.
							$L_{\text{div}}$ (mm)	$d_{\text{throat}}$ (mm)	A/A*			
Ag	15-50	Air	1-2	250-450	-	15	-	-	-	-	SS 347 <sub>grit blasted</sub>	[123]
Al	20	He	1.5-2	20	20	20	-	-	-	~8.3	Al <sub>pickled</sub>	[124]
Al	2-20	-	-	-	10-12	12	-	-	1	1.66	Al	[125]
Al	5-50	N <sub>2</sub>	3.45	230	15	25	168	2	14.21	20	Al2024 T351 <sub>grit blasted</sub>	[126]
Al1100	1-30	He+N <sub>2</sub>	2.1	227-527	-	-	-	-	-	-	Al1100	[127]
Al2618	<25	He	1.7	20	-	15	-	-	-	-	Al <sub>grit blasted</sub>	[128]
Al2618	25-38	He	1.4	20	-	20	-	-	-	8	Al6061 <sub>grit blasted</sub>	[114]
Al7075	-	N <sub>2</sub>	1.6	500	3(rpm)	15	-	2	9.9	20	Al5052 <sub>grit blasted</sub>	[73]
Al	15	He	0.62	200	15	12	-	-	-	0.83	AZ91 Mg	[129]
Al	1-40	Air	1.6	230	-	20	-	2x4	1.375	10	AZ91D <sup>3</sup> <sub>sandblasted</sub>	[130]
Al 101	6-174	He	0.98	300	-	10	-	-	10	-	AZ91D-T4 <sub>grit blasted</sub>	[131]
Al	40; 60; 80	Air	2	204-371	-	20	80	3	~2.8	-	Brass <sub>sandblasted</sub>	[132]
Al	~80	Air	0.7-2.5	280	-	10	-	1	49	-	Ni	[133]
Al	15-75	He	2.5	20	10	20	-	-	-	27	Sn Hv=0.08 GPa Cu Hv=0.95 GPa Al 6063 Hv=0.97 GPa Brass Hv=1.10 GPa Hv=2.18 GPa BS B01 <sup>4</sup> Hv=6.22 GPa Hv=8.05 GPa SS 1040 Hv=2.33 GPa Al <sub>2</sub> O <sub>3</sub> Hv=10.7 GPa	[17]
Cu	-	N <sub>2</sub>	1.5	300	-	20	-	-	-	10	Al6061 <sub>polished</sub>	[78]

<sup>2</sup> Transverse rate

<sup>3</sup> Magnesium alloy

<sup>4</sup> Chromium-tungsten-steel tool

Cu	5-25	He	3	20	4(rpm)	20	1.35	~8.8	100	Al6082 pickled	[134]
Cu <sup>5</sup>	75	Air	2.5	500	-	30	-	3.8	100	Cu grit blasted	[135]
Cu	1.32	He	-	-	-	-	-	-	-	Cu grit blasted	[136]
Cu	1-50	N <sub>2</sub>	2.7	600	33.3	40	-	-	20	Cast iron	[137]
Cu	5-15	Air	3	300	-	20	50	2	500	SS 400 grit blasted, polished	[64]
Cu	5, 10; 15	Air	0.4-1	250-650	-	-	130	2	4	SS AISI 304 polished Al 6063 polished	[96]
Cu	5,15	He	0.2-1	20 ; 400	-	-	130	2	4	SS AISI 304 400° C - polished	[138]
Inconel 625	38-15	N <sub>2</sub>	3.2-3.3	500	-	-	-	-	-	SS 304 grit blasted	[139]
Inconel 718	33	N <sub>2</sub>	3.5	800	23.7	60	-	-	100	Mild steel grit blasted	[140]
Ni	5-22	N <sub>2</sub>	3	600	-	-	-	-	-	Steel grit blasted	[141]
SS 304	52	N <sub>2</sub>	3	450-550	80	25	-	-	-	Steel IF <sup>6</sup>	[142]
	18-25			500						Al	[143]
	28-45			600	Gaz flow rate of 8m <sup>3</sup> /h	50	-	-	-	Al	[144]
	36-53			720						Al	[145]
SS 316L	20-40	N <sub>2</sub>	2-4	600-800	33	40	-	-	500	Al7075 T6 pickled	[146]
Ta	10-30	N <sub>2</sub>	3.8	800	-	40	-	-	333.3	Al cleaned Steel grit blasted	[147]
Ti	-	N <sub>2</sub>	2.7	370-480	1.5- 3rpm	5-20	-	-	-	Al grit blasted	[148]
Ti	22	He	1.5	600	6	-	-	-	-	Al 6063 T5	[149]
Ti	25	N <sub>2</sub>	2.5	450	-	-	-	2.7	-	Al <sub>2</sub> O <sub>3</sub>	[13]
Ti	38-44	N <sub>2</sub>	2	155-263	-	15	100	2	9	Mild steel sandblasted	[147]
		He	1	255	-						[147]
Ti	<25	He	2.9	20	5	20	100	1.35	500	Iron polished Mild steel polished	[91]
Ti	44	N <sub>2</sub>	2	450	-	15	100	2	80	SS 304 polished 1Cr13 <sup>7</sup> SS sandblasted	[148]
Ti	29	N <sub>2</sub>	3; 4	300-800	-	-	-	-	-	Ti	[149]

<sup>5</sup> Preheated powder (25, 100, 200 et 300°C)

<sup>6</sup> IF: interstitial free

<sup>7</sup> Martensitic steel

Ti	16; 22	N <sub>2</sub>	2.4	600	6	20-100	-	-	-	100	Ti	[150]
	16	He	1.5	600		20					Ti	
Ti	5-29	He	1.6	260	-	12	90	3.8	1.1	40	Ti6Al4V grit blasted	[151]
Zn	17; 45	He	2	260	-	-	-	-	-	-	Al6061 grit blasted	[27]
		N <sub>2</sub>	2	320	-	20	100	2	9	600	Zn polished	
Zn	5.2-26.4	He	0.5	140	-	20	100	2	9	80	Mild steel grit blasted	[152]
		N <sub>2</sub>	2	165-410								
Al2319	<63.8					10					Mild steel sandblasted	
Ti	<38.9	Air	2.8	250	-	10	170	2.7	4.9	200	Mild steel sandblasted	[153]
Cu	<98.5					10-30					Mild steel sandblasted	
Al	36			33-500						2	Steel 33-330°C grit blasted	
Zn	13	N <sub>2</sub>	0.6	33-500	-	10	-	-	-	2	Steel 33-245°C grit blasted	[95]
Sn	10			33-80						2	Steel 33-80°C grit blasted	
Al	53-75	Air	2	315	18; 30 24; 72	20	-	2.8	~3.3	25-150	Al	[154]
Zn	45-90									5-150	Al	
Al	10-53	He	2	20	-	90	100	2	1	-		
		N <sub>2</sub>	3	300	-	50	-	2.7	-	-		
Ti	10-50	He	2	20	-	90	100	2	1	-		[155]
		N <sub>2</sub>	3	300	-	50	-	2.7	-	-		
Cu	11-38	He	2	20	-	90	100	2	1	-		
		N <sub>2</sub>	3	300	-	150	-	2.7	-	-		
Al	9-40	Air	1.5-2	290-340	65-87	19-38	-				Al	
											Bronze	
Fe	≤45	Air	1.5-2	480-590	36-55	19-38	-	2.8	2.55	-	Al	[110]
											Bronze	
Cu	≤45	Air	1.5-2	480-590	73-113	19-38	-				Al	
											Bronze	
Cu	10-33	N <sub>2</sub>	1	150	5-10	30	-	2.6	-	0	Cu	[156]
											316L SS	
Ni	10-33	N <sub>2</sub>	1	150	5-10	30	-	2.6	-	0	Cu	
Cu	15-37	N <sub>2</sub>	2	220	-	15	100	2	9	80	SS sandblasted	[157]

Ti	37-44			240														SS polished	
SS 316L	16-44	He	1.5-3	150-300														SS 304 grit blasted	
Iron 101	15-44	N <sub>2</sub>	1-3	200-300	20	20	-	-	-	200								SS 304 grit blasted	
Ti	-	N <sub>2</sub>																-	
Nb	-	N <sub>2</sub>	3	700-850														-	
SS 316	30	N <sub>2</sub>																-	
Al	-	N <sub>2</sub>		300														-	
Cu	-	N <sub>2</sub>	3	300														-	
Ni	-	N <sub>2</sub>		600														Cu, SS, Al	
Ti	5-45	Air	2.8	250	-	30	170	2.7	4.9	-								Mild steel grit blasted	
		N <sub>2</sub>	2	263	-	15	100	2	9	80								Mild steel grit blasted	
Ti6Al4V	5-90	Air	2.8	520	-	30	170	2.7	4.9	-								Mild steel grit blasted	
Al	5-63	Air	2.8	520	-	30	170	2.7	4.9	-								Mild steel grit blasted	
Metals alloys																			
Al-12Si <sup>8</sup>	5-65	He	3	500	-	10	-	-	-	-								Al6061T6 grit blasted	
Al-5Sn	20	He;N <sub>2</sub>	0.7	300	-	10				30								Steel grit blasted	
Al-5Sn	20	N <sub>2</sub>	3	500	-	40			1.56	40								Al6061	
Al-10Sn	15	He;N <sub>2</sub>	0.7	300	-	10				30								Mild steel grit blasted	
Al-10Sn	15.2																		
Al-20Sn	13.8	He;N <sub>2</sub>	0.7	300	25-30	10	-	-	1.56	100								Cu pickled, Al6061 pickled, SUS304 pickled	
Al-13Co-26Ce	23	He	1.7	200-370	-	10	-	2	10; 13	-								Al grit blasted	
Cu-3Ag-0.5Zr	27	He	1.6-2.6	~500	50-61	25	-	2.7	-	5								AlSi4130 grit blasted	
CuCrAl	10-25	He	1.5-2.5	300-500	20-40	5-25	-	-	-	-								GRCop-84 <sup>9</sup>	
Cu-Sn	48	He	2	520	-	30	100	2	5	80								SS sandblasted	
Cu-6Sn	28																		
Cu-8Sn	17	Air	3	500	-	30	170	6	3.83	-								Mild steel	
Diamalloy <sup>10</sup>	<50	N <sub>2</sub>	3.8	800	40.3	20	-	-	-	250								Mild steel polished	
Ti <sub>2</sub> AlC	25-40	N <sub>2</sub>	3.4-3.9	500-800	6	20	-	-	-	50								Al6060	

<sup>8</sup> Preheated at 150°C,<sup>9</sup> Copper alloy with high melting temperature (Cu-8 (at.%) Cr-4% Nb),<sup>10</sup> Diamalloy 4060NS : Chromium-cobalt alloy (Co-28Cr-4W-3Ni-3Fe-1.5Si-1C-1Mo)

600-800										10	Steel grit blasted	
Ceramics and oxides												
Al <sub>2</sub> O <sub>3</sub>	0.5	Air	0.4	20	-	1-7 <sub>40kPa</sub> <sup>11</sup>	5	1x1	3	-	Al <sub>2</sub> O <sub>3</sub>	[172]
SiC	6-33	Air	0.6-0.8	280	-	10	-	-	-	10-25	Inconel 625 cleaned	[23]
WO <sub>3</sub>	30-50	He	0.7	300	-	5	-	4x6	-	-	Si	[6]
Polymers												
PPA	150-250	Air	0.075	20	20-45	10-15	200	5.2	1	-	HDPE	[40]
MCrAlY systems												
CoNiCrAlY	5-37	He	2	550	-	-	270	2	13.3	-	Al6061 grit blasted	[173]
MCrAlY-Re	10-40	N <sub>2</sub>	4	800	~33	30	-	-	-	900	Ni cleaned	[174]
Cermets												
WC-12Co	9; 13; 17	N <sub>2</sub>	2.4	750	-	20	100	2	9	3	SS sandblasted WC-12Co	[44]
WC-12Co	10-30	N <sub>2</sub>	3	800	-	<20	-	-	-	250	Al7075T6 polished Al7075T6 polished	[46]
WC-12Co	15-45	N <sub>2</sub>	4.4	700	40(rpm)	10	-	-	-	10	SS SUS 304 grit blasted	[175]
WC-17Co	15-45	He	3.4	600	30(rpm)	15	-	-	-	10	SS SUS 304 grit blasted	[175]
WC <sup>12</sup> -17Co	~30	He	1.2-1.5	600	36(rpm)	20	-	-	-	60	SS cleaned	[47]
WC-25Co	32	N <sub>2</sub>	3-4	800	-	10-40	-	-	-	250	Al7075-T6 polished Steel polished	[45]
WC-CoCr	34±17	He	1.7	550	-	-	-	-	-	-	Al grit blasted	[43]

<sup>11</sup> Deposition under vacuum condition ( $P_0=0.04\text{MPa}$ )

<sup>12</sup> Two grain size cases for the WC: 2-3 $\mu\text{m}$  and 40-800nm

## A2. Composites-based deposits

Deposit	Powders and ratio (%)	$d_p$ ( $\mu\text{m}$ )	gas	$P_0$ (MPa)	$T_0$ ( $^{\circ}\text{C}$ )	Q (g/mn)	SoD (mm)	Nozzle parameters			$V_{\text{nozzle}}$ (mm/s)	Injection condition	Substrate	Ref.
								$L_{\text{div}}$ (mm)	$d_{\text{throat}}$ (mm)	A/A*				
Al/Cu	Cu (50) Al (50)	5-25 15-45	He	1.5; 2.9	-	60	20	100	~1.35	~8.8	500	Mixing <sub>30mn</sub> and injection	Cu cleaned	[176]
Al/Cu	Al (10,20) Cu (20,10)	5-45 5-45	N <sub>2</sub>	1.72	350	-	10	-	-	-	20	Mixing and injection	-	[177]
Al/Fe	Fe (50) Al (50)	54 74	N <sub>2</sub>	2	350	-	20	100	2	9	40	Grinding <sub>30mn</sub> and injection	SS sandblasted	[178]
Al/Ni	Al (75) Ni (25)	77 43	Air	0.8	280	-	10	-	-	49	-	Mixing <sub>30mn</sub> and injection	Al	[179]
Al/Ti	Ti (25)	3											Al	
Al/Ti	Al (50) Ti (50)	10-45 45	He	1.6	100; 200	20	10	80	-	78.5	33.33	Mixing and injection	Al grit blasted	[180]
Al/Al <sub>x</sub> Ni <sub>y</sub>	Al (75;90) Ni (25;10)	~77 ~3	Air	0.8	280	-	10	-	1	-	-	Mixing <sub>30mn</sub> and injection	Al	[181, 182]
Al/ Mg <sub>17</sub> Al <sub>12</sub>	Al (50-25) Mg <sub>17</sub> Al <sub>12</sub> (50-75)	<45 48.5	He	1.03	300	-	10	-	-	-	1	Mixing <sub>30mn</sub> and injection	AZ91D Mg grit blasted	[183]
Al/Al <sub>2</sub> O <sub>3</sub>	Al (90;10) Al <sub>2</sub> O <sub>3</sub> (10;90)	≤44 50-100	Air	0.7	330	-	5	-	-	24	-	Mixing and injection	Al6061 Si	[184]
Al/Al <sub>2</sub> O <sub>3</sub>	Al (7-75) Al <sub>2</sub> O <sub>3</sub> (-)	80-180 25.5	N <sub>2</sub>	0.62	560	8-12	10	-	-	-	2	Mixing and injection	Al7075 grit blasted Steel grit blasted	[185]
Al/Al <sub>2</sub> O <sub>3</sub>	Al <sub>2</sub> O <sub>3</sub> (15-75 <sub>vol</sub> )	10 20	He	0.62	65; 125	-	12	-	-	1	100	Mixing <sub>1h</sub> and injection	AZ91 Mg cleaned	[186]
Al/Al <sub>2</sub> O <sub>3</sub>	Al <sub>2</sub> O <sub>3</sub> (25-75 <sub>vol</sub> )	15 20	He	0.62	125	15	12	-	-	1	0.83	Mixing <sub>1h</sub> and injection	AZ91E Mg cleaned	[187]
Al/Al <sub>2</sub> O <sub>3</sub>	Al (75,50) Al <sub>2</sub> O <sub>3</sub> (25,50)	1-30	Air	1.6	230	-	30	-	2x4	5	10	Mixing and injection	AZ91 Mg grit blasted	[188]
Al/Al <sub>2</sub> O <sub>3</sub>	(1:10, 10:1)	<50	Air	0.7	330	-	5	-	-	24	-	As-purchased	Si	[189]
Al/SiC	(1:10, 10:1)	<50	Air	0.7	330	-	5	-	-	24	-	As-purchased		

Al /CuO	Al (2:3)	$\frac{4.1}{<20}$	He	1.4-1.7	150	11	10-15	100	2	9.61	10	Mixing et injection	SS 4130 <sub>grit blasted</sub>	[190]
	Al (2:3)	$\frac{4.1}{45-53}$	He	1.4-1.7	150	11	10-15	100	2	9.61	10	Mixing and injection	SS 4130 <sub>grit blasted</sub>	
Al/Zn	Al (40;60)	53-75	Air	2	315	24; 30	20	-	2.8	~3.3	25-38	Mixing and injection	Al	
	Zn (60;40)	53-90												
Al/Zn/Si	Zn (17;51)	53-90	Air	2	315	30	20	-	2.8	~3.3	25-102	Mixing and injection	Al	[154]
	Al (68;34)	53-75												
Al-Si/ Zn	Si (15;15)	40-50	Air	2	315	30	20	-	2.8	~3.3	25-102	Mixing and injection	Al	
	Zn (6-70)	45-90												
Al-12Si /SiC	Al-Si(94-30)	53-75	He	1.7-3	360-500	2	10	-	-	-	-	Mixing and injection	Al6061T6 <sub>grit blasted</sub>	[191, 192]
	Al-12Si (-)	5-45												
Al/ Al-Si/CNT	SiC (20-60)	<32	He	2.9	-	-	-	-	-	-	-	Mixing <sub>1h</sub> and injection	Al6061 <sub>pickled</sub>	[81]
	Al (80;90)	~26												
Al2319/ TiN	CNT (0.5;1)	~57	Air	2.6	490	-	20	170	-	4.9	-	Mixing and injection	Al <sub>sandblasted</sub>	[193]
	Al2319 (50)	5-63												
Al7075 /B <sub>4</sub> C	TiN (50)	10-45	He	0.98	300	-	10	-	-	-	1	Mixing and injection	Al6061T6 <sub>cleaned</sub>	[194]
	Al7075 (80)	15												
Al7075 /SiC	B <sub>4</sub> C (20)	7	He	0.98	300	-	10	-	-	-	1	Mixing and injection	Al6061T6 <sub>cleaned</sub>	
	Al7075 (90)	15												
CuSn8 /AlCuFeB	SiC (10)	28	Air	3	500	-	30	-	-	-	-	Mixing and injection	Mild steel	[195]
	CuSn8 (50)	17												
CuSn8 /TiN	AlCuFeB (50)	17	Air	3	500	-	30	-	-	-	-	Mixing and injection	Mild steel	
	CuSn8 (50)	17												
Cu/CNTs	TiN (50)	25	N <sub>2</sub>	3.5	200	5 <sub>cm3/mn</sub>	35	-	-	-	10	Prior mixing and injection	Cu	[83]
	ratio of CNTs (5 - 15)	~40												
Fe/Al	2.8	500	N <sub>2</sub>	2	510	-	15	100	2	9	40	Grinding and injection	Steel <sub>sandblasted</sub>	[196]
	Al (40)	74												
HA-Ag/ PEEK	Fe (60)	54	Air	1.1-1.2	150-160	-	15	-	-	-	50	Mixing <sub>24h</sub> and injection	Glass <sub>cleaned</sub>	[197]
	HA-Ag (20-80)	$\frac{<45}{<45}$												

HA <sup>13</sup> /Ti	HAP (20,50) Ti (80,50)	-	N <sub>2</sub>	3.5	700	2(rpm)	15	-	-	-	-	Mixing and injection	Ti grit blasted	[198]
Mg/Ti	Ti (-) Mg (75)	10-45 63-73	He	1	340	-	-	-	-	-	-	Mixing and injection	Ti	[199]
Ni/Al	Ni (50) Al (50)	20 42	He	2.1	178	-	-	-	-	-	-	Mixing and injection	Al6061T6	[200]
Ni/Al/ MoO <sub>3</sub>	Ni (70,65) Al (25,25) MoO <sub>3</sub> (5,10)	20 42 27	He	2.1	174-176	-	-	-	-	-	-	Mixing and injection	Al6061T6	[200]
Ni/Al <sub>2</sub> O <sub>3</sub>	Ni (~60) Al <sub>2</sub> O <sub>3</sub> (~40)	61-100	Air	2.7	495	15-20	30	170	-	4.9	160	Mixing and injection	Mild steel sandblasted	[201]
Ni/Al <sub>2</sub> O <sub>3</sub>	Ni (60) Al <sub>2</sub> O <sub>3</sub> (40)	10-50 25	Air	1.8-2	650	-	30	-	4x2	2.5	10	Mixing and injection	Inconel cleaned	[202]
Ni/B <sub>4</sub> C	Ni B <sub>4</sub> C (25-65)	35 35 140	N <sub>2</sub>	3	600	10	20	-	-	-	300	Mixing <sup>24h</sup> and injection	AISI 316L	[203]
NiO/Al <sub>2</sub> O <sub>3</sub>	NiO (-) Al <sub>2</sub> O <sub>3</sub> (-)	<75	N <sub>2</sub>	1.4	500	-	20	62.6	1.55	3	5	Mixing and injection	SS polished, pickled	[42]
NiCrAl /CBN <sup>14</sup>	NiCrAl (-) CBN (40)	5-65	He	2.2	600	18.4	20	100	2	9	15	Mixing and injection	SS grit blasted	[204]
Sn/Ni	Sn (70,50) Ni (30,50)	60 40	Air	0.7-2	330	-	10	-	1	49	-	Mixing and injection	Ni Cu	[205]
SS316 /Al <sub>2</sub> O <sub>3</sub>	Al <sub>2</sub> O <sub>3</sub> (25-75)	7 20	He	6.2	320	15	12	-	-	1	0.83	Mixing <sup>30mn</sup> and injection	AZ91 Mg	[206]
SS316L /Cr-Co	SS 316L (-) Cr-Co (25:33)	24 33	N <sub>2</sub>	4	700	20	80	-	-	-	300	Mixing <sup>1h</sup> and injection	Mild steel grit blasted	[207]
Ti/Al	Al (32) Ti (68)	10-53 50-150	He	2	20	30	50	-	2	-	50	Mixing <sup>30mn</sup> and injection	-	[208]

<sup>13</sup> HA : Hydroxyapatite<sup>14</sup> Cubic bore nitride

TiAl <sub>3</sub> /Al	TiAl <sub>3</sub> (1:3)	$\frac{25-37}{25-37}$	Air	1.8	250	-	10	-	-	-	-	Mixing <sup>48h</sup> and injection	Ti <sub>2</sub> AlNb polished	[209]
W/Cu	W (75) Cu (25)	$\frac{<1}{<45}$	75 N <sub>2</sub>	37.27	-	-	10	-	3	2.22	-	Grinding and injection	Mild steel	[210]
WC-12Co /Ni	WC (50-96) Ni (50-4)	$\frac{15-45}{-}$	Air	6.34	550	60	5	-	4.46	~2	5	Mixing and injection	Mild steel sandblasted	[211, 212]
Zn/Al	Zn (70) Al (30)	$\frac{<10}{<30}$	N <sub>2</sub>	2.4	400	-	20	-	-	-	-	Mixing <sup>1h</sup> and injection	Mild steel	[213]
Zn-Fe /TiO <sub>2</sub>	Zn-Fe (-) TiO <sub>2</sub> (-)	$\frac{180-500}{-}$	Air	0.4-0.6	20	-	50-130	-	-	-	-	-	SS 400 polished Cu polished	[214]
Al/Cu	Al Cu	$\frac{28}{39}$	N <sub>2</sub>	1.5	300	$\frac{18}{30}$	-	20	3	~4.7	10	Separate injection <sup>15</sup>	Al	[71]
Al/Cu	Al (60) Cu (40)	$\frac{28}{39}$	N <sub>2</sub>	2	427	-	200	20	3	~4.7	-	Separate injection	Al sandblasted Steel sandblasted	
Al/Ti	Ti (50) Al (50)	$\frac{36}{28}$	N <sub>2</sub>	2	550	-	200	20	3	~4.7	-	Separate injection	Al sandblasted Steel sandblasted	
Al/Al <sub>2</sub> O <sub>3</sub>	Al (50) Al <sub>2</sub> O <sub>3</sub> (50)	$\frac{28}{25}$	N <sub>2</sub>	3	227	-	200	20	3	~4.7	-	Separate injection	Al sandblasted Steel sandblasted	
Al/SiC	Al (50) SiC (50)	$\frac{28}{38}$	N <sub>2</sub>	3	227	-	200	20	3	~4.7	-	Separate injection	Al sandblasted Steel sandblasted	[69]
Cu/Al <sub>2</sub> O <sub>3</sub>	Cu (50) Al <sub>2</sub> O <sub>3</sub> (50)	$\frac{39}{25}$	N <sub>2</sub>	3	427	-	200	20	3	~4.7	-	Separate injection	Al sandblasted Steel sandblasted	
Cu/SiC	Cu (50) SiC (50)	$\frac{39}{38}$	N <sub>2</sub>	3	427	-	200	20	3	~4.7	-	Separate injection	Al sandblasted Steel sandblasted	
Ti/SiC	Ti (50) SiC (50)	$\frac{36}{38}$	N <sub>2</sub>	3	600	-	200	20	3	~4.7	-	Separate injection	Al sandblasted Steel sandblasted	

<sup>15</sup> Subsonic injection of the Cu powders (at the nozzle inlet) and supersonic injection of the Al powders (50mm from the throat location)

**A3. Nanostructured deposits using nanocrystalline powders**

Powder	$d_p$ ( $\mu\text{m}$ )	gas	$P_0$ (MPa)	$T_0$ ( $^{\circ}\text{C}$ )	$Q$ (g/mn)	SoD (mm)	Nozzle parameters			$V_{\text{nozzle}}$ (mm/s)	Substrate	Ref.
							$L_{\text{div}}$ (mm)	$d_{\text{throat}}$ (mm)	A/A*			
Al5083 <sub>nc</sub> <sup>16</sup>	<45	He	1.7	20	-	-	180-270	2	9-13.3	-	Al <sub>grit blasted</sub>	[74]
Al7075 <sub>nc</sub>	-	N <sub>2</sub>	1.7	500	3(rpm)	15	-	2	9.9	20	Al5052 <sub>grit blasted</sub>	[73]
Cu <sub>nc</sub> <sup>17</sup>	-	N <sub>2</sub>	2	300	-	10	-	-	-	5	Al6061 <sub>polished</sub>	[78]
Ni <sub>nc</sub> <sup>15</sup>	<53	He	1.7	5	-	12 <sub>0.8MPA</sub>	-	-	-	-	Al <sub>grit blasted</sub>	[79]
NiCrAlY <sub>nc</sub>	52	He	2.5	500	-	(15)	100	2	9	-	Inconel 738	[80]
WC <sub>nc</sub> <sup>18</sup> -12Co	~20 <sup>19</sup>	He	3	600	30	15	-	-	-	10	SUS 304 <sub>grit blasted</sub>	[215]
WC <sub>nc</sub> <sup>20</sup> -12Co	5-44	He	2	600	-	20	100	2	4	-	SS <sub>sandblasted</sub>	[216]
WC15-Co <sub>nc</sub>	37±22	He	1.7	550	-	-	-	-	-	-	Al <sub>grit blasted</sub>	[43]

<sup>16, 17</sup> Grain size of 20-30nm<sup>17</sup> Grain mean size of 32nm<sup>18</sup> Grain size of 100-200nm<sup>19</sup> Preheated at 500 $^{\circ}\text{C}$ <sup>20</sup> Grain size of 50-500nm

## A4. Nanoporous deposits using nanosized powders

Powder	$d_p$ ( $\mu\text{m}$ )	gas	$P_0$ (MPa)	$T_0$ ( $^{\circ}\text{C}$ )	$Q$ (l/mn)	SoD (mm)	Nozzle parameters			$V_{\text{nozzle}}$ (mm/s)	Substrate	Ref.
							$L_{\text{div}}$ (mm)	$d_{\text{throat}}$ (mm)	A/A*			
TiN <sub>ns</sub>	0.02-0.03	He	$1^{-4}$ - $7^{-3}$	20	-	6	-	2.5x0.25	-	$5_{0.2-7\text{kPa}}$ <sup>21</sup>	$\alpha$ -Al <sub>2</sub> O <sub>3</sub> cleaned	[65]
TiO <sub>2ns</sub>	0.025	He	1	20	-	5	-	-	-	$5_{0.23\text{kPa}}$ <sup>22</sup>	FTO glass cleaned	[10]
TiO <sub>2ns</sub>	$\frac{0.025}{0.200}$	He	1	20	-	5	-	2.5x0.2	-	$5_{2\text{kPa}}$ <sup>22</sup>	$\frac{\text{SS}}{\text{ITO glass cleaned}}$	[12]
TiO <sub>2np</sub>	10-45 <sup>22</sup>	N <sub>2</sub>	2	300	-	10	100	2	9	500	SS sandblasted	[217]
TiO <sub>2np</sub>	0.5-3 <sup>23</sup>	He	0.1	20	3-7.5	10	-	2.5x0.2	-	$5_{<2\text{kPa}}$ <sup>22</sup>	FTO glass	[35,87]
TiO <sub>2ns</sub> /PEG	<1	He	-	-	3	5	-	2.5x0.2	-	$5_{2\text{kPa}}$ <sup>22</sup>	glass	[66]

<sup>21</sup> Deposition under vacuum condition<sup>22</sup> Nanoporous powder<sup>23</sup> Nanoporous powder prepared by a primary TiO<sub>2</sub><sub>25nm</sub>-PEG mixture + PEG removal by a post heat treatment

nc: nanocrystalline, np: nanoporous, ns: nanosized

## A5. MMCs deposits with nanosized phases

Deposit	Powders and ratio (%)	d <sub>p</sub> (μm)	gas	P <sub>0</sub> (MPa)	T <sub>0</sub> (°C)	Q (g/mn)	SoD (mm)	Nozzle parameters			V <sub>nozzle</sub> (mm/s)	Injection condition	Substrate	Ref.
								L <sub>div</sub> (mm)	d <sub>throat</sub> (mm)	A/A*				
CNTs/Al /Al-Si	Al (80;90)	~26	He	2.9	-	-	-	-	-	-	-	Mixing <sup>1h</sup> and injection	Al6061 pickled	[81]
	Al-Si (-) CNT (0.5;1)	~57												
Al <sub>ns</sub> /Ni	Ni (50)	4.2	He	1	300	11	10	-	-	-	1	Mixing <sup>40mn</sup> and injection	Al	[77]
	Al (50)	6.8												
CNTs/Cu	CNTs (3)	-	Air	0.6	-	-	-	0.5-0.6 MPa <sup>24</sup>	-	4.8	-	Mixing <sup>20h</sup> and injection	Al	[82]
	Cu (-)	0.5-3												
CNTs/Cu	CNTs (5-15)	~40	N <sub>2</sub>	3.5	200	5 <sub>cm3/mn</sub>	35	-	-	-	10	Mixing <sup>4h</sup> and injection	Cu	[83]
	Cu (-)	2.8		500										
ND <sup>25</sup> /Al	ND(10)	~28	N <sub>2</sub>	1.72	450	-	-	-	-	-	-	Mixing <sup>0.5;3h</sup> and injection	Steel 1018 grit blasted	[84]
	Al(-)													
TiN/SiC	TiN (10; 30; 50)	0.02 0.04	He	0.01	20	-	3-9 <sub>0.1kPa</sub> <sup>23</sup>	-	2.5x0.25	1-5	Wet milling, drying, injection	α-Al <sub>2</sub> O <sub>3</sub> cleaned	[218]	

<sup>24</sup> Deposition under vacuum condition<sup>25</sup> Nanodiamond with a size of 30-200nm  
ns: nanosized

## 46. Hybrid deposit/substrate combinations

Powder	$d_p$ ( $\mu\text{m}$ )	gas	$P_0$ (MPa)	$T_0$ ( $^{\circ}\text{C}$ )	$Q$ (g/min)	SOD (mm)	Nozzle parameters				$V_{\text{nozzle}}$ (mm/s)	Substrate	Ref.	
							$L_{\text{div}}$ (mm)	$d_{\text{throat}}$ (mm)	$A/A^*$					
Metal/glass, metal/ceramic														
Al	15-75	He	2.5	20	10	20	-	-	-	-	-	27	ABS HV=0.17 GPa	[17]
Al	15; 30	$\text{N}_2$	1-2.4	100-300	-	20	~ 90	-	10.7	50	LZT cleaned	50	Glass HV=4.45 GPa	[19]
Ti	25	$\text{N}_2$	2.5	450	-	-	-	2.7	-	-	$\text{Al}_2\text{O}_3$	-	-	[13]
Cu	0.5-1.5	Air	0.6	330	3	55	100	6	2.15	35	Glass cleaned, Si cleaned	35	-	[18]
Metal/polymer, metal/PMCs														
Al	15-45	$\text{N}_2$	1.2	300	5	20	-	3.8	4.21	5	CFRCs	-	-	[26]
Cu	<30	$\text{N}_2$	2.5	-	116.6	30	130	-	-	-	HDPE, PP, PTFE, PC, Nylon 6, PU	-	-	[28]
Cu	5-20	$\text{N}_2$	1-3	20-400	5(rpm)	30	-	-	-	-	PVC, epoxy	-	-	-
Cu dendritic	5-45	$\text{N}_2$	1-3	20-400	5(rpm)	30	-	-	-	~8.3	PVC, epoxy	-	-	[20,21]
Sn	5-20	$\text{N}_2$	1-3	20-400	5(rpm)	30	-	-	-	-	PVC, epoxy	-	-	-
Cu	10-32	$\text{N}_2$	0.5-3	20	5-18(rpm)	40	180	2	9	~8-16	PC/ABS GFRCS	-	-	[25]
Sn	10-32	$\text{N}_2$	3	20	200(rpm)	103	70	2	9	14	PC/ABS, PP, PS, PA	-	-	[25]
Ti	20-90	$\text{N}_2$	-	-	-	-	-	-	-	-	PEEK	-	-	[39]
Zn	17,45	He	1-3	250-400	-	-	-	-	-	-	CFRCs	-	-	[27]
Oxide/polymer														
$\text{TiO}_2$	45-60	$\text{N}_2$	1.5-3	400-550	5-10	30	-	2.7	9.7	80-100	PEEK, PET, PVDF, PSU, PES, PPSU	-	-	[22]
$\text{TiO}_2$	<1	Air	0.7	20	~7-15	$1.5_{20-40}\text{ka}^{26}$	-	0.590	-	0.05	PMMA, PET	-	-	[37]
Polymer/Metal														
PPA	150	Air	0.075	20	28	15	200	5.2	1	-	Al $110^{\circ}\text{C}-140^{\circ}\text{C}$	-	-	[40]
PE	53-75	Air	0.583	275	-	12	-	9.8	-	-	Al7075T6	-	-	[29]
Cermets/metal, ceramic/metal														

<sup>26</sup> Deposition under vacuum condition

WC-12Co	9; 13; 17	N <sub>2</sub>	2.4	750	-	20	100	2	9	3	SS sandblasted WC-12Co	[44]
WC-12Co	10-30	N <sub>2</sub>	3	800	-	<20	-	-	-	250	Al7075T6 polished	[46]
WC-12Co	15-45	N <sub>2</sub>	4.4	700	40(rpm)	10	-	-	-	10	SS SUS 304 grit blasted	[175]
WC-17Co	15-45	He	3.4	600	30(rpm)	15	-	-	-	10	SS SUS 304 grit blasted	[47]
WC <sup>27</sup> -17Co	~30	He	1.2-1.5	600	36(rpm)	20	-	-	-	60	SS cleaned	[45]
WC-25Co	32	N <sub>2</sub>	3-4	800	-	10-40	-	-	-	250	Al7075-T6 polished Steel polished	[43]
WC-CoCr	34±17	He	1.7	550	-	-	-	-	-	-	Al grit blasted	[42]
NiO-Al <sub>2</sub> O <sub>3</sub>	<75	N <sub>2</sub>	1.4	500	-	20	62.6	1.55	3	5	SS polished, pickled	[23]
SiC	6-33	Air	0.6-0.8	280	-	10	-	-	-	10-25	Inconel 625 cleaned	[37]
TiO <sub>2</sub>	<1	Air	0.7	20	~7-15	1.5 <sub>20-40kPa</sub> <sup>28</sup>	-	0.910	-	0.05	AISI304 Al, Cu	[38]
Other combination												
HA	-	Air	0.7-2	200-400	10	30	-	1	24	-	PEEK	[219]

<sup>27</sup> Two grain size cases for the WC: 2-3µm and 40-800nm

<sup>28</sup> Deposition under vacuum condition